

---

# Practical Deep Heteroskedastic Regression

---

Mikkel Jordahn <sup>\*1</sup> Jonas Vestergaard Jensen <sup>\*1</sup> James Harrison <sup>2</sup> Michael Riis Andersen <sup>1</sup> Mikkel N. Schmidt <sup>1</sup>

## Abstract

Uncertainty quantification (UQ) in deep learning regression is of wide interest, as it supports critical applications including sequential decision making and risk-sensitive tasks. In heteroskedastic regression, where the uncertainty of the target depends on the input, a common approach is to train a neural network that parameterizes the mean and the variance of the predictive distribution. Still, training deep heteroskedastic regression models poses practical challenges in the trade-off between uncertainty quantification and mean prediction, such as optimization difficulties, representation collapse, and variance overfitting. In this work we identify previously undiscussed fallacies and propose a simple and efficient procedure that addresses these challenges jointly by post-hoc fitting a variance model across the intermediate layers of a pretrained network on a hold-out dataset. We demonstrate that our method achieves on-par or state-of-the-art uncertainty quantification on several molecular graph datasets, without compromising mean prediction accuracy and remaining cheap to use at prediction time.

## 1. Introduction

Uncertainty quantification (UQ) is of wide interest in the field of deep learning due to its utility in several applications, ranging from sequential decision making to safety-critical use-cases (Springenberg et al., 2016; Chitta et al., 2019; Li et al., 2024; Brunzema et al., 2025; Cinquin et al., 2025; Duran-Martin et al., 2025). Bayesian neural networks (BNNs) (MacKay, 1992; Neal, 1995) offer a framework for uncertainty quantification, and while their focus is on the epistemic uncertainty, they can also account for input-dependent aleatory uncertainty when combined with an appropriate observation model. However, when the primary goal is to obtain well-calibrated predictive uncertainty, this can be achieved more directly through heteroskedastic re-

gression (Nix & Weigend, 1994), in which the network is trained to directly output the mean and variance corresponding to the total uncertainty. While the distinction between aleatoric and epistemic uncertainty is a common topic in the literature (Gal, 2016), Smith et al. (2025) argues that separating the two is not practical or necessarily required. We therefore focus on heteroskedastic regression as a means of modeling total uncertainty in large deep learning models, where training costs are high and where mean estimates cannot be compromised upon.

We specifically evaluate our method on molecular regression tasks (Scalia et al., 2020; Busk et al., 2021; Wollschläger et al., 2023; Jiang et al., 2024), predicting energy and other quantum chemical properties of atomistic systems from 3D molecular geometries using large-scale equivariant graph neural networks that have shown strong empirical performance (Qu & Krishnapriyan, 2024; Wood et al., 2025). Here, fast and reliable uncertainty quantification is key, e.g. for molecular simulation or discovery. Yet we find that many of the core problems related to training these models still remain unaddressed.

We identify four core problems with training heteroskedastic regression neural networks, some of which have been discussed in previous works but have not, to the best of our knowledge, been addressed jointly (Skafte et al., 2019; Stirn & Knowles, 2020; Seitzer et al., 2022; Stirn et al., 2023; Wong-Toi et al., 2024). In this work, we propose a practical algorithm for training heteroskedastic regression neural networks that addresses all four problems, and outperforms all other baselines in terms of uncertainty quantification.

The four problems that we identify and analyse with training over-parametrised heteroskedastic regression neural networks with negative log-likelihood and a Gaussian predictive distribution are:

1. Optimisation issues.
2. Last-layer representation collapse.
3. Residual variance overfitting.
4. Practicality.

The method we propose draws upon several works and research areas within deep learning and addresses all four problems jointly. The contributions of this work can thus be

<sup>1</sup>Technical University of Denmark <sup>2</sup>Google DeepMind. Correspondence to: Mikkel Jordahn <mikkjo@dtu.dk>.

summarised as:

- (i) We explicitly identify and characterise four core problems in deep heteroskedastic regression.
- (ii) We propose training (ensembles of) linear variance heads across latent representations using hold-out data, which addresses the identified problems jointly.
- (iii) We show that our proposed method outperforms all compared methods in terms of uncertainty quantification on molecular property prediction datasets using graph neural networks.

## 2. Deep Heteroskedastic Regression Fallacies

**Preliminaries** In the regression setting, we generally have an i.i.d. dataset  $\mathcal{D} = \{(x_i, y_i)\}_{i=1}^N$  where  $x \in \mathbb{R}^d$  is some input and  $y \in \mathbb{R}$  is the output. From this dataset we want to learn a function estimator  $f_\theta$ , which we can use to predict future  $y^*$  given a new  $x^*$ , i.e.  $y^* = f_\theta(x^*)$ . In many applications, it is of interest to have an uncertainty estimate on the predicted  $y^*$ , and in this work we concern ourselves with the *heteroskedastic* uncertainty assumption, meaning that uncertainties are input-dependent. Most commonly, this is done using a Gaussian predictive distribution, such that  $p_\theta(y^*|x^*) = \mathcal{N}(y^*|\mu_\theta(x^*), \sigma_\theta^2(x^*))$ . Nix & Weigend (1994) is the first work accredited with using neural networks to parametrise such a fully input-dependent predictive distribution, a task now known as *deep heteroskedastic regression*. We will refer to neural networks outputting these parameters as *mean-variance networks*. Importantly, throughout this work we assume that we are in the over-parametrized neural network regime, as is generally the case in deep learning applications today.

In the following we further elaborate on the four identified problems and the existing literature in deep heteroskedastic regression on solutions to these fallacies when applicable. We additionally draw on other existing deep learning literature to motivate and develop our method.

### 2.1. Optimisation Issues

The first problem in deep heteroskedastic regression concerns optimization difficulties that arise for gradient-based maximum likelihood-methods. At a basic level, this phenomenon can be understood by inspecting the gradients of the Gaussian negative log-likelihood (NLL) with respect to  $\mu_\theta(x)$  and  $\sigma_\theta^2(x)$ . The NLL loss for the mean-variance network is

$$\mathcal{L}(\theta, \mathcal{D}) = \frac{1}{2} \sum_{(x,y) \in \mathcal{D}} \left[ \log \sigma_\theta^2(x) + \frac{(y - \mu_\theta(x))^2}{2\sigma_\theta^2(x)} \right], \quad (1)$$

and the gradients are

$$\nabla_{\mu_\theta(x)} \mathcal{L} = \sum_{(x,y) \in \mathcal{D}} \frac{y - \mu_\theta(x)}{\sigma_\theta^2(x)}, \quad (2)$$

$$\nabla_{\sigma_\theta^2(x)} \mathcal{L} = \frac{1}{2} \sum_{(x,y) \in \mathcal{D}} \frac{\sigma_\theta^2(x) - (y - \mu_\theta(x))^2}{2\sigma_\theta^4(x)}. \quad (3)$$

Here we see that if the predicted variance for a datapoint  $x$  grows large during training, the updates to both  $\mu_\theta(x)$  and  $\sigma_\theta^2(x)$  slow down. Previous works argue that this often causes mean-variance networks trained this way to produce inaccurate mean predictions and inflated variances. For more details, we refer to Seitzer et al. (2022), who present a thorough analysis of the general optimisation issues encountered when training mean-variance networks end-to-end.

Several works have discussed possible solutions to this problem. Seitzer et al. (2022) propose  $\beta$ -NLL which applies a variance-reweighting term  $\sigma_\theta^{2\beta}(x)$  to the NLL, where  $\beta$  is a hyperparameter. Skafte et al. (2019) propose to first train only the mean of the network and then move to *mean-variance split training* where they alternate between optimizing  $\mu_\theta(x)$  and  $\sigma_\theta^2(x)$ , which requires tuning the warm-up period for  $\mu_\theta(x)$ . Wong-Toi et al. (2024) posit that proper regularization of the mean-variance network may resolve these issues, and propose a reparameterization of the regularization parameters, which directly allows controlling how heavily  $\mu_\theta(x)$  and  $\sigma_\theta^2(x)$  are regularized independently. Takahashi et al. (2018) and Skafte et al. (2019) both argue that a Student’s t parametrization stabilizes these optimisation issues. Finally, a number of works argue for Bayesian approaches, in which a prior is placed on the predictive variance (Stirn & Knowles, 2020; Harrison et al., 2025). Common to most of these methods is that they introduce hyperparameters that require additional tuning, and empirically often come at the cost of degraded mean estimation.

To our knowledge, the *faithful* approach of Stirn et al. (2023) is the only method that preserves mean estimation while resolving these optimisation issues with no tuning cost. This is achieved by detaching the gradients of the variance predictor from the computational graph, such that the uncertainty prediction does not affect the learning of the backbone of the network, and by rescaling the gradient of  $\mu_\theta(x)$  by  $\sigma_\theta^2$  such that the learning of the mean estimator is equivalent to regular mean-squared error. We find that the idea of fully decoupling mean and variance estimation is the most suitable approach for the setting we consider, although it must be combined with additional techniques to address the remaining challenges.

### 2.2. Last-Layer Representation Collapse

Representation collapse refers to the phenomenon where training a neural network end-to-end leads to a compression

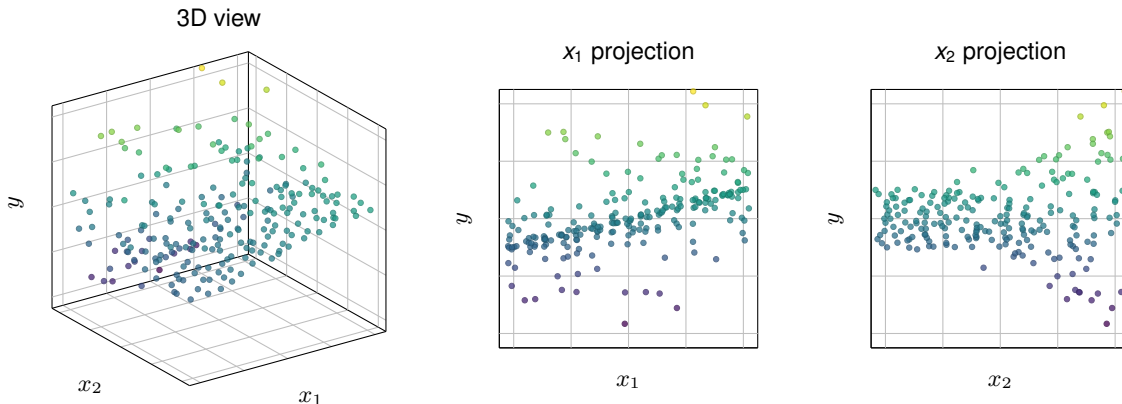


Figure 1. Illustrative plot of data where  $x_1$  dimension fully explains  $\mu(x)$ , whilst  $x_2$  fully explains  $\sigma(x)$ . (Left): 3D View of data distributed with  $y = ax_1 + bx_2^2\epsilon$  with  $\epsilon \sim \mathcal{N}(0, 1)$ . (Middle): Projection of  $y$  onto  $x_1$  where mean increases but variance is constant. (Right): Projection of  $y$  onto  $x_2$  where variance of data increases, but mean remains constant. If only estimating mean  $a$ , it is sufficient to look at only  $x_1$  and a basis function learner can thus completely ignore  $x_2$ .

in the deeper latent representations, such that distances on the data manifold are no longer preserved. This means that the network may primarily retain information relevant to its mean predictions, potentially compromising tasks that rely on distance information. This has recently been discussed in the context of uncertainty quantification (Van Amersfoort et al., 2020; Liu et al., 2022; Mukhoti et al., 2022; Jimenez & Katzfuss, 2025b;a). Some works propose to regularize the latent representations such that they remain distance *aware* or *preserving* with respect to distances on the data manifold; however, this requires modifying the training process.

In the regression setting, we hypothesise that representation collapse may be particularly pronounced when the variance function of the mean-variance network is not allowed to affect the learning of latent representations such as in Stirn et al. (2023)’s *faithful* approach. Intuitively, directions on the data manifold along which the predicted mean  $\mu_\theta(x)$  does not vary may be eliminated by the network during mean-only learning. In other words, the latent representation learned for predicting the mean may not span the subspace of directions relevant for predicting the variance.

To make this precise, let the data  $\mathcal{X}$  lie on a manifold  $\mathcal{M}$ , and assume there exists ground-truth target functions  $\mu : \mathcal{M} \rightarrow \mathbb{R}$  and  $\sigma : \mathcal{M} \rightarrow \mathbb{R}$  which can be exactly decomposed as

$$\mu(x) = H(h(x)), \quad \sigma(x) = G(g(x)), \quad (4)$$

where  $h : \mathcal{M} \rightarrow \mathcal{H}$  and  $g : \mathcal{M} \rightarrow \mathcal{G}$  are nonlinear embeddings,  $\mathcal{H}$  and  $\mathcal{G}$  are minimal latent vector spaces, and  $H : \mathcal{H} \rightarrow \mathbb{R}$ ,  $G : \mathcal{G} \rightarrow \mathbb{R}$  are (generalized) linear models. This corresponds to neural networks with non-linear backbones and linear output layers. If we first learn  $\mu_\theta(x) = H_\theta(h_\theta(x))$  and use the latent representation  $h_\theta(x)$  learned for  $\mu$  to predict the variance,  $\sigma$  can be exactly represented only if  $\mathcal{G} \subseteq \mathcal{H}$ . In Figure 1 we provide a simple,

illustrative example of data where this is not the case.

This issue could for example be relevant for molecular properties such as atomic positions in crystal structures: While the mean positions remain essentially constant with increasing temperature, the variance grows due to thermal vibrations. If a latent representation is learned solely to predict the mean, it may fail to capture these variance-only directions, leading to poor uncertainty estimates.

We now explain why representation collapse is a larger problem for models that decouple location and scale, such as heteroskedastic Gaussian regression, compared with models that do not, such as binary classification.

*Binary classification:* Consider a neural network  $z_\theta(x) : \mathbb{R}^d \rightarrow \mathbb{R}$ , trained with binary cross entropy loss and a sigmoid activation. Suppose  $z_\theta(x)$  is  $L$ -Lipschitz,

$$|z_\theta(x) - z_\theta(x')| \leq L\|x - x'\|. \quad (5)$$

Let  $x_0$  be a point on the decision boundary,  $z_\theta(x_0) = 0$ . For any point  $x$  at distance  $r = \|x - x_0\|$  from the boundary the network output satisfies

$$|z_\theta(x)| \leq Lr \Rightarrow 1 - s \leq p(y = 1|x) \leq s, \quad (6)$$

where  $s = \sigma(Lr)$  and  $p(y = 1|x) = \sigma(z_\theta(x))$ . This shows that the smoothness of the neural network directly bounds the classifier’s confidence, forcing it to express uncertainty in between classes. The same reasoning applies to any probabilistic models where location and scale are not decoupled: Smoothness of the mean function constrains the predictive uncertainty.

*Heteroskedastic Gaussian regression:* In contrast, consider neural networks  $\mu_\theta(x), \sigma_\theta(x) : \mathbb{R}^d \rightarrow \mathbb{R}$ , parameterizing the mean and variance of a Gaussian. Here the predictive uncertainty is determined solely by  $\sigma_\theta(x)$ . Crucially, smoothness of  $\mu_\theta(x)$  or  $\sigma_\theta(x)$  does not constrain the uncertainty

that can be expressed. Therefore, even smooth networks can experience representation collapse without a corresponding increase in predicted uncertainty, making models with decoupled location and scale particularly vulnerable.

### 2.3. Residual Variance Overfitting

As part of learning an uncertainty output, it is necessary to estimate residuals on target labels. This presents an issue in the overparametrised deep learning setting due to the double descent phenomenon (Belkin et al., 2019; Nakkiran et al., 2019; Belkin et al., 2020), where training points are almost perfectly interpolated. The double descent literature generally shows that test error improves even upon, and beyond, completely interpolating all training data points where the training error approaches 0. In this setting, it is to be expected that residuals estimated on the training points, will not generalise well, an issue that is often ignored in the UQ literature for regression. Based on this we argue that all uncertainty quantification methods require an independent hold-out dataset for calibration, which leads us to ask if learning the variance function directly on the same hold-out dataset is possible in this regime.

### 2.4. Practicality

The final issue we identify relates to the practicality of previously presented methods, specifically cast in the light of training large-scale neural networks. We argue that a practical method for this setting should: (i) Retain mean precision compared to a non-heteroskedastic model. (ii) Not require hyperparameter tuning on the full training dataset. (iii) Not incur large prediction time costs. (iv) Have a low implementation barrier. Previous works in deep heteroskedastic regression do not fulfill criteria (i) and (ii) due to mean estimates being harmed (Stirn et al., 2023) and introducing additional hyperparameters at training time. Post-hoc methods, on the other hand, *do* fulfill criteria (i) and (ii) for practicality, which is why we argue that the post-hoc paradigm is the most promising for our setting.

## 3. Method

In this work, we propose a method for uncertainty estimation in deep learning models for regression tasks, which is inspired by diverse areas of deep learning literature, that addresses the core problems identified in training neural networks for heteroskedastic regression. Specifically, we propose learning a linear variance head predictor *post hoc* on a hold-out dataset whilst keeping the mean predictor, and by extension, backbone, fixed. A central piece to our method is to use one or more intermediate *latent representations* (denoted  $z^l$ ) as inputs to the linear variance head predictor, rather than the last latent representation  $z^L$  only (Kristiadi et al., 2020; 2022; Stirn et al., 2023).

The general form for this linear variance head predictor is

$$\sigma_\phi^2(x^*) = \text{sp} \left( \sum_{l \in L_\sigma} W_l^T z^l(x^*) \right), \quad (7)$$

i.e. a sum of linear projections on the latent representations  $z^l$  learnt during mean estimator training. Here  $L_\sigma$  indicates the layers chosen for inputs to the variance head and  $\text{sp}$  is the softplus function. The parameters  $\phi = \{W_l^T\}_{l \in L_\sigma}$  are learnt using the NLL loss in Eq. (1) on hold-out data, with a fixed mean estimator  $\mu_\theta(x)$  learnt on training data. Generally, we use the notation  $\sigma_l^2(x)$  to denote the uncertainty estimator learnt with  $L_\sigma = \{l\}$ , i.e., on the  $l$ 'th latent representation only and  $\sigma_{L_\sigma}^2(x)$  to denote the estimator learnt on all latent representations, i.e., with  $L_\sigma = \{1, 2, \dots, L\}$ .

Whilst simple, our method addresses all of the previously identified problems of deep heteroskedastic regression jointly. We address optimisation issues by fitting the variance head post hoc and independently from the mean estimator. Whilst this could introduce the representation collapse issue as described in Sec. 2.2, our method mitigates this problem by utilising intermediate latent representations for the uncertainty predictor as has been done in previous works (Jimenez & Katzfuss, 2025b). Next, our method resolves the issue of underestimated residuals described in Sec. 2.3 by directly learning the uncertainty estimator on hold-out data where (benign) overfitting has not occurred. Finally, the method fulfills the practicality criteria described in Sec. 2.4, as it does not require interventions at training time nor interferes with mean estimator, only requires a normal forward pass at prediction time with minimal additional parameter cost and is easy to implement as it only requires writing a `hook` in PyTorch (Ansel et al., 2024) to extract latent representations and use a linear layer on top of these.

As an additional variation to our method, we propose ensembling the uncertainty estimators independently learnt on single latent representations. Specifically, we form the predictive distribution as a Gaussian mixture given by

$$p(y^*|x^*) = \frac{1}{|L_\sigma|} \sum_{l \in L_\sigma} \mathcal{N}(y^*|\mu_\theta(x^*), \sigma_l(x^*)^2), \quad (8)$$

where we emphasize that all components have the same mean. We propose this modification as prior work consistently indicates that ensembles can improve performance by reducing variance (Batchelor & Dua, 1995; Krogh & Sollich, 1997), in this case at a minimal additional cost.

## 4. Experiments

We conduct a series of experiments, focusing on molecular regression tasks, to showcase that our proposed method is able to obtain good uncertainty estimates compared to baselines, despite its simplicity. We also show that the latent

Table 1. Test mean absolute errors (MAE) and negative log-likelihoods (NLL) on the QM9 dataset for baseline methods and our post-hoc variance ensemble. Results are averages over three seeds with best results highlighted in bold font. The standard error of the mean is reported in parenthesis in the unit of the last significant digit.

Target	MAE ↓						NLL ↓					
	Homo. NLL	Naïve NLL	Nat. NLL	$\beta$ -NLL	Faithful	Post-hoc (Ensemble)	Homo. NLL	Naïve NLL	Nat. NLL	$\beta$ -NLL	Faithful	Post-hoc (Ensemble)
$\alpha$	0.077 (51)	0.044 (0)	0.045 (0)	<b>0.043 (0)</b>	0.050 (1)	0.077 (51)	-0.412 (280)	-1.36 (10)	-1.29 (4)	<b>-1.40 (1)</b>	-0.665 (61)	-1.04 (59)
$\epsilon_{\text{HOMO}}$	26.6 (2)	25.4 (4)	25.8 (3)	<b>25.3 (4)</b>	26.7 (4)	26.6 (2)	-1.69 (1)	-1.94 (5)	-1.91 (4)	-1.92 (4)	-1.72 (10)	<b>-1.96 (1)</b>
$\epsilon_{\text{LUMO}}$	19.1 (2)	19.1 (2)	19.0 (2)	<b>18.9 (3)</b>	19.2 (2)	19.1 (2)	-2.00 (1)	-2.28 (2)	-2.26 (3)	-2.27 (4)	-1.85 (24)	<b>-2.30 (2)</b>
$\Delta\epsilon$	43.4 (4)	43.6 (8)	43.2 (5)	<b>42.8 (7)</b>	43.4 (2)	43.4 (4)	-1.29 (0)	-1.42 (2)	-1.43 (1)	-1.43 (2)	-1.34 (2)	<b>-1.48 (1)</b>
ZPVE	1.28 (2)	1.25 (1)	1.23 (1)	<b>1.23 (0)</b>	1.28 (2)	1.28 (2)	-4.15 (9)	-4.81 (5)	-4.92 (5)	-4.95 (4)	-4.12 (9)	<b>-4.97 (3)</b>
$U_0$	5.64 (8)	5.89 (12)	99.2 (138)	<b>5.48 (5)</b>	5.62 (8)	5.64 (8)	-2.85 (2)	-2.93 (8)	-0.429 (401)	-2.86 (26)	-2.32 (40)	<b>-3.46 (4)</b>
$U$	<b>5.59 (15)</b>	6.00 (24)	74.3 (53)	5.78 (13)	5.64 (10)	5.59 (15)	-2.84 (3)	-2.86 (18)	-0.849 (56)	-2.88 (9)	-2.60 (37)	<b>-3.45 (3)</b>
$H$	5.61 (12)	6.01 (23)	93.8 (57)	<b>5.56 (9)</b>	5.64 (14)	5.61 (12)	-2.85 (4)	-2.85 (34)	-0.655 (59)	-2.93 (9)	-1.92 (86)	<b>-3.46 (4)</b>
$G$	7.21 (12)	7.55 (11)	75.5 (99)	<b>7.11 (18)</b>	7.21 (4)	7.21 (12)	-2.74 (3)	-2.84 (1)	-0.667 (335)	-2.90 (8)	-1.48 (120)	<b>-3.16 (4)</b>
$c_v$	0.024 (0)	0.024 (0)	0.024 (0)	<b>0.024 (0)</b>	0.024 (0)	0.024 (0)	-1.91 (1)	-2.02 (1)	-1.98 (0)	-2.03 (1)	-1.91 (2)	<b>-2.04 (1)</b>

representation chosen for variance prediction has a large impact on the efficacy of the uncertainty estimates. We additionally present a range of sensitivity experiments to validate the robustness of our method. Finally, we show that these results generalize to large-scale state-of-the-art machine learning interatomic potentials trained on OMol25.

**Datasets and models** We experiment on the QM9 dataset (Wu et al., 2018) using the PaiNN graph neural network (Schütt et al., 2021) and on the OMol25 dataset using FAIR’s UMA model (Wood et al., 2025) and the AllScAIP model (Qu & Krishnapriyan, 2024; Qu, 2025). Both the UMA model and the AllScAIP model are trained on 100 million molecules from the OMol25 dataset (Levine et al., 2025) while UMA is additionally trained on OMat24 (Barroso-Luque et al., 2024), OC20 (Chanussot et al., 2021), ODAC25 (Sriram et al., 2025), and OMC25 (Gharakhanyan et al., 2025). The QM9 and OMol25 settings highlight two different scenarios; one where the model can be trained from scratch at a modest compute budget and one where it is highly impractical to retrain the models to obtain uncertainty estimates, necessitating a reliable post-hoc procedure.

**Baselines** In the QM9 experiment, we benchmark our method against homoskedastic regression and heteroskedastic regression using a naïve Gaussian negative log-likelihood (Naïve NLL), a Gaussian NLL using the natural parameterisation (Natural NLL) (Immer et al., 2024),  $\beta$ -NLL (Seitzer et al., 2022), and Faithful heteroskedastic regression (Faithful) (Stirn et al., 2023). All of these methods learn a mean and variance function jointly on the training data, while ours only learn a variance function on a hold-out dataset. To enable a fair comparison, we fit a constant scaling factor for the baselines’ variance functions on the hold-out data to improve calibration as proposed in Levi et al. (2020) — we note that without this, the NLLs of the end-to-end trained models are extremely poor (App. B). We additionally tune the  $\beta$  parameter for  $\beta$ -NLL on the hold-out data.

In the OMol25 experiments, training from scratch with the previous methods is infeasible, and we are therefore limited to a comparison against homoskedastic regression, where the variance scale is again learnt on hold-out data. The OMol25 experiments are conducted to showcase that the results from the QM9 dataset generalises to larger models and datasets and that we can equip large-scale models with useful uncertainty estimates in a practical way without significant computational overhead. For additional training details, we refer to App. A.

#### 4.1. QM9

In our first experiment, we train the baseline methods on the QM9 dataset end-to-end and recalibrate the resulting variance functions on the hold-out data with a constant scaling factor. As our goal is to obtain useful uncertainty estimates while retaining the predictive performance of the mean, we early-stop training based on the mean absolute error (MAE) on the hold-out data for all methods. Our post-hoc method is learnt on top of the homoskedastic model using the ensemble approach in Eq. (8) with hold-out data. The variance functions  $\sigma_l(x)^2$  are learnt on all five latent representations of the PaiNN architecture, i.e., we use  $L_\sigma = \{0, 1, \dots, 4\}$  in Eq. (8), where  $z^4$  is the last layer representation.

In Table 1, we see that all methods achieve similar MAE on the test data with  $\beta$ -NLL achieving slightly better means on most targets. Although, the MAE results are generally similar, we note that Natural NLL performs considerably worse on the targets  $U_0$ ,  $U$ ,  $H$ , and  $G$ , which is due to the natural parameterisation’s sensitivity to the scale of the data. In the NLL comparison, we see that our post-hoc variance ensemble achieves the best mean performance on all targets except  $\alpha$ , although this is likely due to a poor mean fit of the homoskedastic model. Across all targets our method is at least on-par with existing end-to-end methods, but also often superior. To summarize, our post-hoc variance ensemble

retains predictive performance (in terms of the MAE) while offering at least competitive, but often better, NLLs. In App. B we provide additional results and analysis of the models trained on QM9.

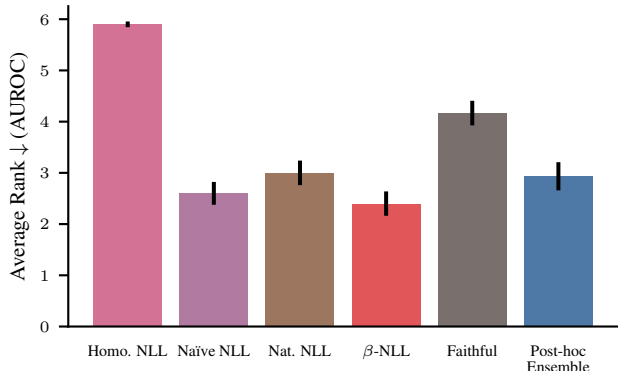


Figure 2. QM9 OOD detection rankings for baseline methods and our post-hoc variance ensemble using the AUROC metric. Rankings are computed for every combination of target and seed and averaged. Error bars indicate the standard error of the mean.

**Out-of-Distribution Detection** We additionally examine the methods’ out-of-distribution behavior by evaluating the learned variance functions’ ability to discriminate between in-distribution datapoints (QM9) and out-of-distribution (OOD) datapoints. We use a subset of the test split of the Alchemy dataset (Chen et al., 2019) as our OOD data and report the FPR95 and AUROC metrics in Table 3 in App. B and average rankings across the QM9 targets for the AUROC metric in Figure 2. We see that our post-hoc variance ensemble ranks slightly worse than some of the baselines. We note that the homoskedastic uncertainty does not have any utility for OOD detection since the predictive uncertainty is constant by design, as can be seen in Figure 2.

**Choice of Latent Representation** In the experiments in Table 1 and Figure 2, we used the ensemble approach described in Section 3. We now examine the utility of each individual uncertainty estimator  $\sigma_l^2(x)$  learnt on individual representations  $z^l(x)$  and the utility of the uncertainty estimator  $\sigma_{L_\sigma}^2(x)$  learnt on all latent representations, i.e.,  $L_\sigma = \{0, 1, \dots, 4\}$ . Figure 3 shows average rankings of these uncertainty estimators across the QM9 targets and seeds according to the NLL metric. Please see App. C for the raw NLL metrics and expected calibration errors (ECE). In Figure 3 we observe that the later latent representations  $z^{\{3,4\}}$ , are never optimal for variance prediction while earlier representations rank much better. This confirms our intuition from Section 2.2 that the model’s last latent representation might not contain the information needed for a useful variance prediction. We also note that fitting a linear model on all of the model’s representations is better than us-

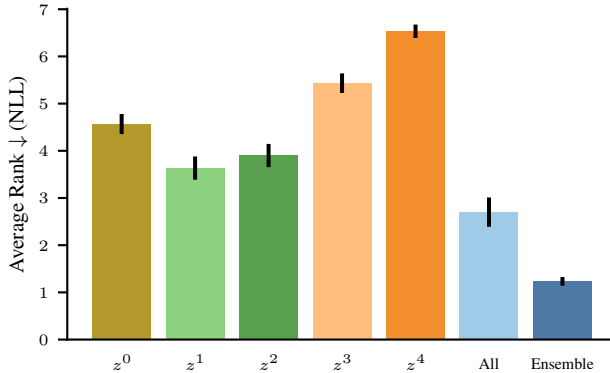


Figure 3. QM9 test NLL rankings of fitting the uncertainty estimator using different individual representations  $z^l$ , all representations, or an ensemble of the individual estimators. Rankings are computed for every combination of target and seed and averaged. Error bars indicate one standard error of the mean.

ing a single representation, but that the ensemble approach is superior to this in terms of NLL, even though these two uncertainty estimators have the same number of parameters.

**Sensitivity to Weight Decay** In Table 1 and Figures 2 and 3, we used the same weight decay factor  $\lambda$  for fitting Eq. (7) as the one used during end-to-end training of the homoskedastic and heteroskedastic baseline models ( $\lambda = 0.01$ ). However, the effect of weight decay may depend on the representation  $z^l$  used. We therefore investigate the different representations’ sensitivity to  $\lambda$  on the QM9 target  $U$  in Figure 4 and for the  $U_0$  target in App. B. In Figure 4 we see that most representations are largely insensitive to  $\lambda$  although a too large  $\lambda$  is detrimental for all representations. We do note that  $z^1$  and the usage of all representations display sensitivity to  $\lambda$  and are unstable for small values of  $\lambda$ , i.e., low levels of regularization. This is, however, not

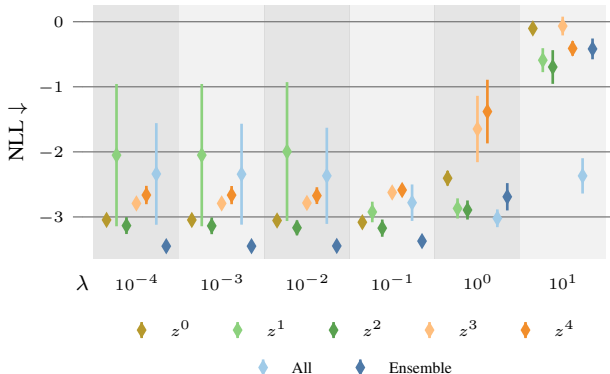


Figure 4. The effect of varying the weight decay parameter  $\lambda$  when fitting the linear uncertainty estimator using different individual representations  $z^l$ , all representations, or an ensemble of the individual estimators. Results are test NLL averages over three seeds on the QM9  $U$  target and are plotted with one standard error.

the case for  $U_0$  (Figure 15 in App. D) where instead the last-layer representation  $z^4$  is unstable. Nonetheless, the post-hoc variance ensemble displays stable behaviour on both targets.

**Hold-Out Dataset Size** Our method naturally depends on the hold-out data used for fitting the variance function, and one might hypothesise that less hold-out data is required to recalibrate end-to-end trained networks. We therefore examine the effect of varying the size of the hold-out data and compare to the baselines. Naturally, the optimal regularization strength depends on the size of the hold-out dataset. Consequently, we do not use weight decay in this setting, but instead employ an early-stopping strategy, which corresponds to using optimised weight decay (Bishop, 1995). For details on this approach see App. A. In Figure 5, we see the test NLL on the QM9  $U$  target as a function of the hold-out dataset size. Here, we observe that the baselines are relatively invariant to the hold-out dataset size but worse for most dataset sizes compared to the post-hoc variance ensemble, whose performance increases with the hold-out dataset size, as expected. Surprisingly, the post-hoc ensemble performs well even for only 200 hold-out datapoints.

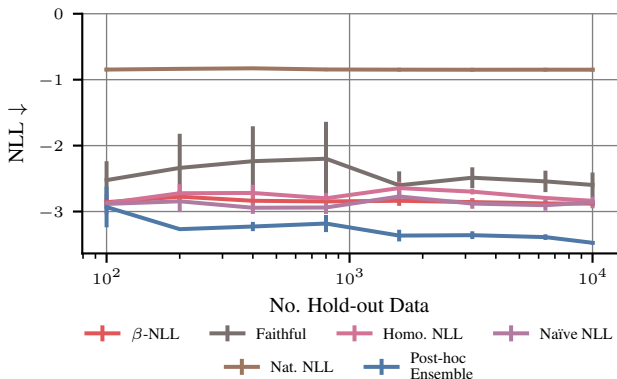


Figure 5. Effect of varying hold-out dataset size. Results are test NLL on the QM9  $U$  target and are averaged over three seeds. Error bars indicate the standard error of the mean.

## 4.2. OMol25

Finally, we evaluate the ability of our post-hoc method to equip large pretrained models with useful uncertainty estimates. We experiment using the smaller variants of the UMA and AllScAIP models. We use three random (but disjoint) subsets of 20,000 datapoints from the OMol25 validation dataset and split each of them into equally sized hold-out and test datasets and report results as averages over the three subsets. In Table 2, we report the test MAE, NLL, and ECE for both UMA and AllScAIP using homoskedastic regression, our post-hoc linear variance predictor using all latent representations, and our post-hoc variance ensemble for energy prediction. The homoskedastic models are the

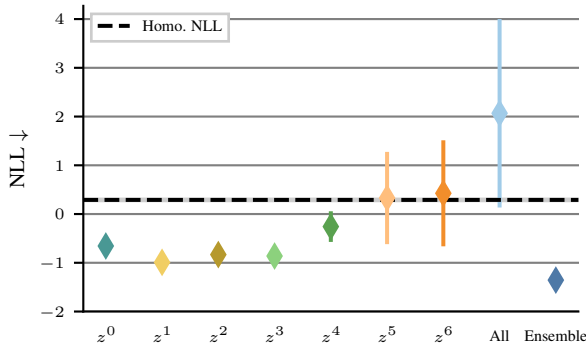


Figure 6. OMol25 test NLL when fitting the linear variance estimator using different individual representations  $z^l$ , all representations, or an ensemble of the individual estimators. Results are averages over three seeds and subsets of the full data. Error bars indicate the standard error of the mean.

pretrained models with a constant variance fitted on the hold-out data. Firstly, we see in Table 2 that the MAEs are equal to those in the official OMol25 leaderboard (Levine et al., 2025) for the chosen models, indicating that our test splits are representative of the full OMol25 validation dataset of  $\approx 2.8$  million molecules. Secondly, we see that the post-hoc variance ensemble outperforms homoskedastic regression by a large margin. We also see that the ensemble performs better than the variance estimator fitted on all representations in terms of NLL but worse in terms of ECE.

Table 2. Test MAE, NLL, and ECE on the OMol25 dataset for homoskedastic regression, the post-hoc linear variance predictor using all latent representations, and the post-hoc variance ensemble fitted on top of the trained UMA and AllScAIP models. Results are averages over three seeds and subsets of the full data with best results highlighted in bold font. The standard error of the mean is reported in parenthesis in the unit of the last significant digit.

Model	MAE ↓	NLL ↓			ECE ↓		
		Homo. NLL	All	Ensemble	Homo. NLL	All	Ensemble
UMA	60.7 (17)	0.290 (39)	2.07 (379)	<b>-1.36</b> (7)	0.209 (9)	<b>0.105</b> (33)	0.133 (15)
AllScAIP	42.2 (3)	-0.354 (103)	-1.59 (45)	<b>-1.94</b> (8)	0.186 (18)	<b>0.025</b> (3)	0.053 (3)

**Choice of Latent Representation** Like for the QM9 experiments in Section 4.1, we investigate the effect of the representations chosen for fitting the linear uncertainty estimator on OMol25. In Figure 6, we show the test NLL for the different individual estimators  $\sigma_l^2(x)$ , the estimator using all latent representations  $\sigma_{L\sigma}^2(x)$ , and the ensemble of the individual estimators as a Gaussian mixture. We observe that the results from QM9 generalizes to the UMA model, i.e., that earlier latent representations are more useful for variance prediction while later ones are worse and more unstable. In contrast, we see in the AllScAIP case in Figure 17 in App. D that most representations provides

uncertainty estimates of similar quality. We do however note that ensembling the individual variance predictors is by far superior in both cases.

**Calibration** We qualitatively investigate the calibration of the post-hoc variance ensemble fitted on top of UMA and AllScAIP. In Figure 7, we observe that the calibration curve for the post-hoc variance ensemble on both UMA and AllScAIP follows the oracle remarkably well<sup>1</sup>. The predictive uncertainty (rank) correlates well with the prediction error on the test data. Whilst not a guarantee for success, such uncertainties are required for effective sequential experimental design pipelines such as active learning and Bayesian optimisation.

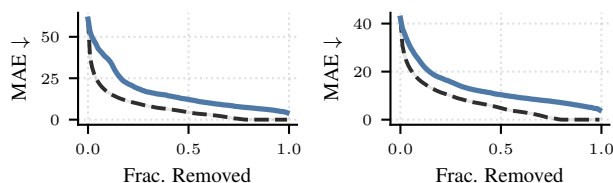


Figure 7. Calibration plots (left): UMA. (right): AllScAIP.

## 5. Discussion

**Performance** We firstly discuss aspects of performance and provide practical recommendations for uncertainty estimation. Throughout the QM9 experiments, we observed that not only did our ensembled post-hoc uncertainty estimators perform on par with end-to-end trained mean-variance networks, they actually in many cases outperformed them. In the ablation studies, we additionally showed that our method is highly robust to different weight decay values, and that even for very small hold-out data set sizes ( $< 1000$  datapoints), the ensembled post-hoc uncertainty estimators performed better than fully end-to-end trained neural networks. This was further illustrated on OMol25 using the UMA and AllScAIP models, where we again observed the highly calibrated uncertain estimates of our ensembled uncertainty predictors. Based on this evidence, we argue that end-to-end training of mean-variance networks is not necessary for effective heteroskedastic uncertainty estimation, as long as one can extract intermediate latent representations.

**End-to-End Training Works** An unexpected observation from our experiments, is that existing end-to-end mean-variance training methods appear to generally work quite well. Whilst the existing literature argue that optimisation issues lie at the core of failure of training these models, we suspect that it may primarily be a temperature scaling issue. Whilst uncalibrated versions of these models exhibit poor NLL, they preserve correct rankings of uncertainties as

evidenced by calibration plots in App. B, and it is possible to recover strong NLL performance simply by rescaling the variance with a temperature estimated from a hold-out dataset. We hypothesise that a common pitfall when training these models may be to early-stop based on, or optimise for, validation NLL, leading to poor mean estimates. Rather than this, the mean component of the model should be allowed to converge followed by temperature rescaling, or alternatively a conformalising procedure (Vovk et al., 2005). It is possible that early-stopping should be rethought in regression as it has been argued for classification by Berta et al. (2025). We leave further investigations of these training dynamics for future work.

**Robust Ensembles vs. Sharp "All" Model** A general observation throughout our work is that depending on the application, the choice of representation used for the variance predictor may change. Specifically, we find that the ensemble variance predictors which yield a Gaussian mixture predictive distribution are more robust to outliers due to their heavier tails which yields better test NLL, and more robustness at small hold-out dataset sizes. However, this comes with the trade-off that ECE and OOD metrics decrease for these models in comparison to the "All" version which has sharper predictions. With this in mind, we argue that whilst the ensembled variance predictors should be used generally, there may be applications where the sharper but less robust "All" variance predictor may be preferred.

**Relation to Previous Works** Although our method directly relates to mean-variance networks, it does carry similarities to (Jimenez & Katzfuss, 2025b). However, their presented method relies on additional hyperparameter choices, incurs inference time costs and have memory requirements that for some applications may be limiting. In contrast, our method does not introduce any additional hyperparameters, incurs minimal memory cost due to a small parameter increase in the model, and incurs essentially no inference time cost as it only requires a regular forward pass. We elaborate more on these differences in App. E.

## 6. Conclusion

In this work, we have identified and analysed the core problems related to training deep learning models for heteroskedastic regression and devised a highly practical method that addresses these problems. We showed that our method often outperforms end-to-end trained mean-variance networks on QM9 and that the method extends to large scale machine learning interatomic-potentials models trained on OMol25. We argue this method paves the way for applications of such large-scale models where good predictive uncertainty is required and can have immense impact, such as in molecular discovery.

<sup>1</sup>For details on how these plots are generated, see Figure 9.

## Impact Statement

This paper presents work whose goal is to advance the field of machine learning. There are many potential societal consequences of our work, none of which we feel must be specifically highlighted here.

## References

- Ansel, J., Yang, E., He, H., Gimelshein, N., Jain, A., Voznesensky, M., Bao, B., Bell, P., Berard, D., Burovski, E., Chauhan, G., Chourdia, A., Constable, W., Desmaison, A., DeVito, Z., Ellison, E., Feng, W., Gong, J., Gschwind, M., Hirsh, B., Huang, S., Kalambarkar, K., Kirsch, L., Lazos, M., Lezcano, M., Liang, Y., Liang, J., Lu, Y., Luk, C., Maher, B., Pan, Y., Puhersch, C., Reso, M., Saroufim, M., Siraichi, M. Y., Suk, H., Suo, M., Tillet, P., Wang, E., Wang, X., Wen, W., Zhang, S., Zhao, X., Zhou, K., Zou, R., Mathews, A., Chanan, G., Wu, P., and Chintala, S. PyTorch 2: Faster Machine Learning Through Dynamic Python Bytecode Transformation and Graph Compilation. In *29th ACM International Conference on Architectural Support for Programming Languages and Operating Systems, Volume 2 (ASPLOS '24)*. ACM, April 2024. doi: 10.1145/3620665.3640366. URL <https://docs.pytorch.org/assets/pytorch2-2.pdf>.
- Barroso-Luque, L., Shuaibi, M., Fu, X., Wood, B. M., Dzamba, M., Gao, M., Rizvi, A., Zitnick, C. L., and Ulissi, Z. W. Open materials 2024 (omat24) inorganic materials dataset and models. *arXiv preprint arXiv:2410.12771*, 2024.
- Batchelor, R. and Dua, P. Forecaster diversity and the benefits of combining forecasts. *Management Science*, 41(1): 68–75, 1995.
- Belkin, M., Hsu, D., Ma, S., and Mandal, S. Reconciling modern machine-learning practice and the classical bias–variance trade-off. *Proceedings of the National Academy of Sciences*, 116(32):15849–15854, July 2019. ISSN 1091-6490. doi: 10.1073/pnas.1903070116. URL <http://dx.doi.org/10.1073/pnas.1903070116>.
- Belkin, M., Hsu, D., and Xu, J. Two models of double descent for weak features. *SIAM Journal on Mathematics of Data Science*, 2(4):1167–1180, January 2020. ISSN 2577-0187. doi: 10.1137/20m1336072. URL <http://dx.doi.org/10.1137/20M1336072>.
- Berta, E., Holzmüller, D., Jordan, M. I., and Bach, F. Re-thinking early stopping: Refine, then calibrate, 2025. URL <https://arxiv.org/abs/2501.19195>.
- Bishop, C. M. *Neural Networks for Pattern Recognition*. Oxford University Press, Inc., USA, 1995. ISBN 0198538642.
- Brunzema, P., Jordahn, M., Willes, J., Trimpe, S., Snoek, J., and Harrison, J. Bayesian optimization via continual variational last layer training. *International Conference on Learning Representations (ICLR)*, 2025.
- Busk, J., Jørgensen, P. B., Bhowmik, A., Schmidt, M. N., Winther, O., and Vegge, T. Calibrated uncertainty for molecular property prediction using ensembles of message passing neural networks, 2021. URL <https://arxiv.org/abs/2107.06068>.
- Chanussot, L., Das, A., Goyal, S., Lavril, T., Shuaibi, M., Riviere, M., Tran, K., Heras-Domingo, J., Ho, C., Hu, W., et al. Open catalyst 2020 (oc20) dataset and community challenges. *Acs Catalysis*, 11(10):6059–6072, 2021.
- Chen, G., Chen, P., Hsieh, C.-Y., Lee, C.-K., Liao, B., Liao, R., Liu, W., Qiu, J., Sun, Q., Tang, J., et al. Alchemy: A quantum chemistry dataset for benchmarking ai models. *arXiv preprint arXiv:1906.09427*, 2019.
- Chitta, K., Alvarez, J. M., and Lesnikowski, A. Large-scale visual active learning with deep probabilistic ensembles, 2019. URL <https://arxiv.org/abs/1811.03575>.
- Cinquin, T., Lo, S., Strieth-Kalthoff, F., Aspuru-Guzik, A., Pleiss, G., Bamler, R., Rudner, T. G. J., Fortuin, V., and Kristiadi, A. What actually matters for materials discovery: Pitfalls and recommendations in bayesian optimization. In *AI for Accelerated Materials Design - ICLR 2025*, 2025. URL <https://openreview.net/forum?id=Gbv2JjfnSY>.
- Duran-Martin, G., Sánchez-Betancourt, L., Cartea, A., and Murphy, K. P. Martingale posterior neural networks for fast sequential decision making. In *The Thirty-ninth Annual Conference on Neural Information Processing Systems*, 2025. URL <https://openreview.net/forum?id=fqfYzp4GKi>.
- Fu, X., Wood, B. M., Barroso-Luque, L., Levine, D. S., Gao, M., Dzamba, M., and Zitnick, C. L. Learning smooth and expressive interatomic potentials for physical property prediction. *arXiv preprint arXiv:2502.12147*, 2025.
- Gal, Y. Uncertainty in deep learning. 2016. URL <https://api.semanticscholar.org/CorpusID:86522127>.
- Gharakhanyan, V., Barroso-Luque, L., Yang, Y., Shuaibi, M., Michel, K., Levine, D. S., Dzamba, M., Fu, X., Gao, M., Liu, X., et al. Open molecular crystals 2025 (omc25) dataset and models. *arXiv preprint arXiv:2508.02651*, 2025.

- Harrison, J., Willes, J., Brunzema, P., and Snoek, J. Heteroscedastic variational last layers. In *7th Symposium on Advances in Approximate Bayesian Inference – Workshop Track*, 2025. URL <https://openreview.net/forum?id=I7PeIAwJ7I>.
- Immer, A., Palumbo, E., Marx, A., and Vogt, J. Effective bayesian heteroscedastic regression with deep neural networks. In *Neural Information Processing Systems (NeurIPS)*, 2024.
- Jiang, S., Qin, S., Van Lehn, R. C., Balaprakash, P., and Zavala, V. M. Uncertainty quantification for molecular property predictions with graph neural architecture search. *Digital Discovery*, 3(8):1534–1553, 2024. ISSN 2635-098X. doi: 10.1039/d4dd00088a. URL <http://dx.doi.org/10.1039/D4DD00088A>.
- Jimenez, F. and Katzfuss, M. Probabilistic skip connections for deterministic uncertainty quantification in deep neural networks, 2025a. URL <https://arxiv.org/abs/2501.04816>.
- Jimenez, F. and Katzfuss, M. Vecchia gaussian process ensembles on internal representations of deep neural networks, 2025b. URL <https://arxiv.org/abs/2305.17063>.
- Kristiadi, A., Hein, M., and Hennig, P. Being Bayesian, even just a bit, fixes overconfidence in relu networks. In *International Conference on Machine Learning (ICML)*, 2020.
- Kristiadi, A., Eschenhagen, R., and Hennig, P. Posterior refinement improves sample efficiency in bayesian neural networks, 2022. URL <https://arxiv.org/abs/2205.10041>.
- Krogh, A. and Sollich, P. Statistical mechanics of ensemble learning. *Physical Review E*, 55(1):811, 1997.
- Levi, D., Gispan, L., Giladi, N., and Fetaya, E. Evaluating and calibrating uncertainty prediction in regression tasks, 2020. URL <https://openreview.net/forum?id=ryg8wpEtvB>.
- Levine, D. S., Shuaibi, M., Spotte-Smith, E. W. C., Taylor, M. G., Hasyim, M. R., Michel, K., Batatia, I., Csányi, G., Dzamba, M., Eastman, P., Frey, N. C., Fu, X., Gharakhanyan, V., Krishnapriyan, A. S., Rackers, J. A., Raja, S., Rizvi, A., Rosen, A. S., Ulissi, Z., Vargas, S., Zitnick, C. L., Blau, S. M., and Wood, B. M. The open molecules 2025 (omol25) dataset, evaluations, and models, 2025. URL <https://arxiv.org/abs/2505.08762>.
- Li, Y. L., Rudner, T. G. J., and Wilson, A. G. A study of Bayesian neural network surrogates for Bayesian optimization. In *International Conference on Learning Representations (ICLR)*, 2024.
- Liu, J., Padhy, S., Ren, J., Lin, Z., Wen, Y., Jerfel, G., Nado, Z., Snoek, J., Tran, D., and Lakshminarayanan, B. A simple approach to improve single-model deep uncertainty via distance-awareness. *Journal of Machine Learning Research*, 2022.
- Loshchilov, I. and Hutter, F. Decoupled weight decay regularization. *arXiv:1711.05101*, 2017.
- MacKay, D. J. A practical bayesian framework for back-propagation networks. *Neural Computation*, 1992.
- Mukhoti, J., Kirsch, A., van Amersfoort, J., Torr, P. H. S., and Gal, Y. Deep deterministic uncertainty: A simple baseline, 2022. URL <https://arxiv.org/abs/2102.11582>.
- Nakkiran, P., Kaplun, G., Bansal, Y., Yang, T., Barak, B., and Sutskever, I. Deep double descent: Where bigger models and more data hurt, 2019. URL <https://arxiv.org/abs/1912.02292>.
- Neal, R. M. *Bayesian Learning for Neural Networks*. PhD thesis, University of Toronto, 1995.
- Nix, D. A. and Weigend, A. S. Estimating the mean and variance of the target probability distribution. In *International conference on neural networks (ICNN)*, 1994.
- Qu, E. AllScAIP GitHub Repository, 2025. URL <https://github.com/EricZQu/fairchem/tree/allscaip>.
- Qu, E. and Krishnapriyan, A. The importance of being scalable: Improving the speed and accuracy of neural network interatomic potentials across chemical domains. *Advances in Neural Information Processing Systems*, 37: 139030–139053, 2024.
- Scalia, G., Grambow, C. A., Pernici, B., Li, Y.-P., and Green, W. H. Evaluating scalable uncertainty estimation methods for deep learning-based molecular property prediction. *Journal of Chemical Information and Modeling*, 60(6):2697–2717, 06 2020. doi: 10.1021/acs.jcim.9b00975. URL <https://doi.org/10.1021/acs.jcim.9b00975>.
- Schütt, K., Unke, O., and Gastegger, M. Equivariant message passing for the prediction of tensorial properties and molecular spectra. In *International Conference on Machine Learning*, pp. 9377–9388. PMLR, 2021.

- Seitzer, M., Tavakoli, A., Antic, D., and Martius, G. On the pitfalls of heteroscedastic uncertainty estimation with probabilistic neural networks. In *International Conference on Learning Representations (ICLR)*, 2022.
- Skafté, N., Jorgensen, M., and Hauberg, S. Reliable training and estimation of variance networks. *Neural Information Processing Systems (NeurIPS)*, 2019.
- Smith, F. B., Kossen, J., Trollope, E., van der Wilk, M., Foster, A., and Rainforth, T. Rethinking aleatoric and epistemic uncertainty, 2025. URL <https://arxiv.org/abs/2412.20892>.
- Springenberg, J. T., Klein, A., Falkner, S., and Hutter, F. Bayesian optimization with robust bayesian neural networks. In Lee, D., Sugiyama, M., Luxburg, U., Guyon, I., and Garnett, R. (eds.), *Advances in Neural Information Processing Systems*, volume 29. Curran Associates, Inc., 2016. URL [https://proceedings.neurips.cc/paper\\_files/paper/2016/file/a96d3afec184766bfeca7a9f989fc7e7-Paper.pdf](https://proceedings.neurips.cc/paper_files/paper/2016/file/a96d3afec184766bfeca7a9f989fc7e7-Paper.pdf).
- Sriram, A., Brabson, L. M., Yu, X., Choi, S., Abdelmaq-soud, K., Moubarak, E., de Haan, P., Löwe, S., Brehmer, J., Kitchin, J. R., et al. The open dac 2025 dataset for sorbent discovery in direct air capture. *arXiv preprint arXiv:2508.03162*, 2025.
- Stirn, A. and Knowles, D. A. Variational variance: Simple, reliable, calibrated heteroscedastic noise variance parameterization. *arXiv preprint arXiv:2006.04910*, 2020.
- Stirn, A., Wessels, H., Schertzer, M., Pereira, L., Sanjana, N., and Knowles, D. Faithful heteroscedastic regression with neural networks. In *Artificial Intelligence and Statistics (AISTATS)*, 2023.
- Takahashi, H., Iwata, T., Yamanaka, Y., Yamada, M., and Yagi, S. Student-t variational autoencoder for robust density estimation. In *Proceedings of the Twenty-Seventh International Joint Conference on Artificial Intelligence, IJCAI-18*, pp. 2696–2702. International Joint Conferences on Artificial Intelligence Organization, 7 2018. doi: 10.24963/ijcai.2018/374. URL <https://doi.org/10.24963/ijcai.2018/374>.
- Van Amersfoort, J., Smith, L., Teh, Y. W., and Gal, Y. Uncertainty estimation using a single deep deterministic neural network. In *International Conference on Machine Learning (ICML)*, 2020.
- Vovk, V., Gammerman, A., and Shafer, G. *Algorithmic Learning in a Random World*. Springer-Verlag, Berlin, Heidelberg, 2005. ISBN 0387001522.
- Wollschläger, T., Gao, N., Charpentier, B., Ketata, M. A., and Günnemann, S. Uncertainty estimation for molecules: Desiderata and methods, 2023. URL <https://arxiv.org/abs/2306.14916>.
- Wong-Toi, E., Boyd, A. J., Fortuin, V., and Mandt, S. Understanding pathologies of deep heteroskedastic regression. In *The 40th Conference on Uncertainty in Artificial Intelligence*, 2024. URL <https://openreview.net/forum?id=n5faLvrsA0>.
- Wood, B. M., Dzamba, M., Fu, X., Gao, M., Shuaibi, M., Barroso-Luque, L., Abdelmaq-soud, K., Gharakhanyan, V., Kitchin, J. R., Levine, D. S., Michel, K., Sriram, A., Cohen, T., Das, A., Rizvi, A., Sahoo, S. J., Ulissi, Z. W., and Zitnick, C. L. UMA: A Family of Universal Models for Atoms. 6 2025.
- Wu, Z., Ramsundar, B., Feinberg, E. N., Gomes, J., Geniesse, C., Pappu, A. S., Leswing, K., and Pande, V. MoleculeNet: A Benchmark for Molecular Machine Learning. 10 2018.

## A. Training & Experimental Details

In this section, we provide details on the experimental setups and training for the experiments in Sec. 4.1 and 4.2. Code is available at [REDACTED].

### A.1. QM9

For training PaiNN on QM9, we generally follow the procedure of Schütt et al. (2021) with a few slight modifications. The QM9 dataset is split into 110,000 training points, 10,000 hold-out points, and 10,381 test points.

**Homoskedastic Regression** We train the homoskedastic regression model using the MSE loss function for 1,000 epochs with a batch size of 100 molecules using the MAE on the hold-out data as an early-stopping criterion. We use the AdamW optimizer (Loshchilov & Hutter, 2017), a weight-decay factor  $\lambda = 0.01$ , an initial learning rate of  $5e-4$  and decrease the learning rate with cosine annealing. We repeat training for three different random initialisations (seeds) for all targets.

**Heteroskedastic Regression** We follow the same procedure as for the homoskedastic model but use either the naïve Gaussian negative log-likelihood, a Gaussian NLL using the natural parameterisation (Immer et al., 2024),  $\beta$ -NLL (Seitzer et al., 2022), and Faithful heteroskedastic regression (Stirn et al., 2023) as the loss function. All methods use the same backbone and the variance head is attached to the last-layer latent representation. For  $\beta$ -NLL, we do a grid search for  $\beta$  for each seed and target with the grid  $\{0.25, 0.5, 0.75, 1\}$  and use the NLL on the hold-out data as a selection criterion (after recalibrating with a constant variance scale factor).

**Post-Hoc Calibration** After fitting the homoskedastic models and the heteroskedastic models, we rescale their variance functions with a constant scale factor  $\gamma > 0$  such that the predictive distribution becomes

$$p(y^*|x^*) = \mathcal{N}(y^*|\mu_\theta(x^*), \gamma\sigma_\theta^2(x^*)). \quad (9)$$

We fit  $\gamma$  using the NLL criterion on the hold-out data with the L-BFGS optimizer and a learning rate of 0.01, a maximum of 100 iterations per step, a history size of 1,000 (for estimating the Hessian), line search, and 1,000 epochs with full batches.

**Post-Hoc Linear Variance Estimators** The post-hoc linear variance estimators in Equation (7) are fitted using the AdamW optimizer for 500 epochs on the hold-out data using an initial learning rate of  $5e-4$  and cosine annealing. The weight-decay factor  $\lambda$  is set to 0.01 except in the weight-decay sensitivity experiment where we vary it in the grid  $\{1e-4, 1e-3, 1e-2, 1e-1, 1e0, 1e1\}$  and the hold-out dataset sensitivity experiment where we set it 0 and use early-stopping instead.

**Post-Hoc Ensemble of Linear Variance Estimators** We do not do any additional training or tuning for the post-hoc variance ensemble as we simply combine the variance estimators fitted using the above approach in a Gaussian mixture model using Equation (8).

**Per Atom Variance Contributions** In the PaiNN architecture, molecular properties are predicted as a sum of atomic contributions, i.e.,

$$\mu_\theta(x) = \sum_{i=1}^{N_x} W_\mu^T z_i^L(x), \quad (10)$$

where  $N_x$  is the number of atoms in the input molecule  $x$ ,  $z_i^L(x) \in \mathbb{R}^{D \times 1}$  is the last layer representation of the  $i$ th atom in  $x$ , and  $W_\mu \in \mathbb{R}^{D \times 1}$ . Similarly, we predict the variance as a sum of atomic contributions in the heteroskedastic models

$$\sigma_\theta^2(x) = \sum_{i=1}^{N_x} \text{sp}(W_\sigma^T z_i^L(x)), \quad (11)$$

where  $\text{sp}$  is the softplus function and  $W_\sigma$  has the same shape as  $W_\mu$ . For our post-hoc linear variance estimators, this equation becomes

$$\sigma_\phi^2(x) = \sum_{i=1}^{N_x} \text{sp} \left( \sum_{l \in L_\sigma} W_l^T z_i^l(x) \right), \quad (12)$$

where  $z_i^l(x)$  is  $l$ th latent representation of atom  $i$  in molecule  $x$ .

**Latent Representations** For the PaiNN architecture, we extract five different latent representations for the different linear variance estimators. We extract the scalar atom representations after each block of message passing and updating as well as the scalar atom representations in the readout MLP. PaiNN has three blocks of message passing and updating, resulting in the representations  $z^{\{0,1,2\}}$ , and a two-layer readout MLP, resulting in the representations  $z^{\{3,4\}}$ , where  $z^4$  is the last-layer representation. We fit variance estimators  $\sigma_l^2(x)$  on each of these individual latent representations, a variance estimator  $\sigma_{L_\sigma}^2(x)$  using all the latent representations ( $L_\sigma = \{0, 1, \dots, 4\}$ ), and combine the individual estimators using Equation (8) in an ensemble.

**Out-of-Distribution Experiment** In the OOD experiments, we use 10,000 datapoints from the test split of the Alchemy dataset (Chen et al., 2019) as OOD datapoints. We then use the learned variance functions  $\gamma\sigma_b^2(x)$  (the baselines),  $\sigma_l(x)^2$ , and  $\sigma_{L_\sigma}^2(x)$  as classifiers to discriminate between ID data (the QM9 test split) and OOD data, and evaluate them using the false positive rate at a 95% true positive rate (FPR95) and the area under receiver operating characteristic curve (AUROC). For the Gaussian mixture model (the ensemble), we have that the variance is

$$\mathbb{V} \left[ \frac{1}{|L_\sigma|} \sum_{l \in L_\sigma} \mathcal{N}(\mu_\theta(x^*), \sigma_l^2(x^*)) \right] = \frac{1}{|L_\sigma|} \sum_{l \in L_\sigma} \sigma_l^2(x^*), \quad (13)$$

due to the component means being equal. We therefore use Equation (13) as the OOD classifier for the post-hoc variance ensemble.

**Hold-Out Dataset Size Experiment** In the experiment investigating the effect of the size of the hold-out dataset, we fit the  $\gamma$  parameter for the baselines as described above but only use the given hold-out subset. For our post-hoc linear variance estimators, we set the weight-decay factor  $\lambda$  to 0 and instead use early-stopping to regularize the models. We do this by further splitting the given hold-out subset into a set used for fitting and one for monitoring the NLL to determine the optimal number of optimization steps, i.e., when to early-stop. When we have found the optimal number of optimization steps, we refit the linear variance estimator using the complete hold-out subset with the found optimal number of steps. We use an 80/20 ratio for this splitting. We use the same optimizer settings as described above but set the maximum number of epochs to 5,000 and use a patience of 50 epochs for the early-stopping.

## A.2. OMol25

**Data** The test split of the OMol25 dataset do not have publicly available labels. Therefore, we use the validation split to create our hold-out and test datasets. We take 10,000 random samples as our hold-out dataset and another 10,000 random samples as our test data to keep computational resources needed for testing manageable. We repeat this process three times, while ensuring there is no overlap between our samples, to get three datasets each with 10,000 hold-out datapoints and 10,000 test datapoints. We report our results as averages over these three datasets. We use the DFT total energy as our target.

**Homeskedastic regression** For the homoskedastic model, we use the pretrained UMA and AllScAIP models as the mean estimator  $\mu_\theta(x)$  and simply fit the variance  $\gamma$  using the hold-out data using the same approach and parameters as when doing post-hoc calibration in the QM9 setup.

**Post-Hoc Linear Variance Estimators** We fit the post-hoc linear variance estimators using the same procedure and parameters as for QM9, with the small addition that we first fit an initial variance scale  $\gamma$  using the same approach as for the homoskedastic model. We do this to help optimization, i.e., not to have variance estimates that are orders of magnitude off at the beginning of optimization. This step is not needed in the QM9 setup as an initial scale is already embedded into the model.

**Per Atom Variance Contributions** The total DFT energy is also predicted as sums of atomic contributions in the UMA and AllScAIP models, and we therefore use Equation (12) again to predict variances.

**Latent Representations** For the UMA model, we extract seven different latent representations. The UMA model is based on the equivariant graph neural network eSEN (Fu et al., 2025). The smaller variant of UMA that we use has 4 blocks of edgewise and nodewise processing, and we extract the atom scalar representations after each of the blocks, resulting in  $z^{\{0,\dots,3\}}$ . The readout MLP of UMA has three layers and we extract the latent representations from this, resulting in the final three representations  $z^{\{4,5,6\}}$ . We use all seven representations in the variance estimator  $\sigma_{L_\sigma}^2(x)$  and in the ensemble model.

The AllScAIP model is an extension of the EScAIP model (Qu & Krishnapriyan, 2024) and is an attention based architecture. We extract eight different latent representations from the model, where the first six representations  $z^{\{0,\dots,5\}}$  are the atom embeddings after each transformer block and the last 2 representations  $z^{\{6,7\}}$  are the atom representations from the two-layer readout MLP. We use all eight representations in the variance estimator  $\sigma_{L_\sigma}^2(x)$  and in the ensemble model.

## B. Additional Results & Analysis on QM9

In this section, we provide additional experimental results and analysis for the methods on QM9. In Figure 8 we provide average rankings of the methods across all targets and seeds for QM9 - lower ranking is better. Here we again see that all methods are comparable in terms of MAE, except for  $\beta$ -NLL which achieves the best MAE on average, which either can be explained by additional regularisation of the mean function, or simply due to the cross validation procedure for the  $\beta$  value, which introduces a slight bias in favor of the  $\beta$ -NLL method. In terms of NLL and ECE on the test data, our post-hoc method achieves the best ranking, whilst several methods are comparable in terms of FPR95. We provide full tables of the OOD metrics for all methods in Table 3.

In Figure 9 we provide calibration plots for each of the methods across the 10 different QM9 targets. We find that most of the methods provide well-ranked uncertainties on most of the targets - as we look at subsets of data that the model are increasingly certain about, the MAE drops as expected. The only models where this is not the case, is the homoskedastic model, which obviously is due to the constant predicted uncertainty and the faithful model which has higher MAEs for more certain subsets. We hypothesise that this may be due to the representation collapse occurring in these models, when the variance head is not allowed to affect the representation learning. Finally, we note that our post-hoc ensemble is the only method that achieves non-constant (and properly calibrated) uncertainties on the  $U_o$ ,  $U$ ,  $H$  and  $G$  targets.

Finally, we provide an analysis of the MAE's and predictive variances on different sized atomic systems. We do this to showcase that the calibration plots are not simply an effect of the variance predictions being a sum over atom representations. We plot MAE and predicted variance as a function of atom count in Fig. 10 and Fig. 11. Here we confirm that MAE and predicted variance are not simply monotonically increasing functions of atom count in the systems, which could give rise to the previously discussed calibration plots, but rather that the uncertainty estimates are heteroskedastic even when controlling for atomic system size.

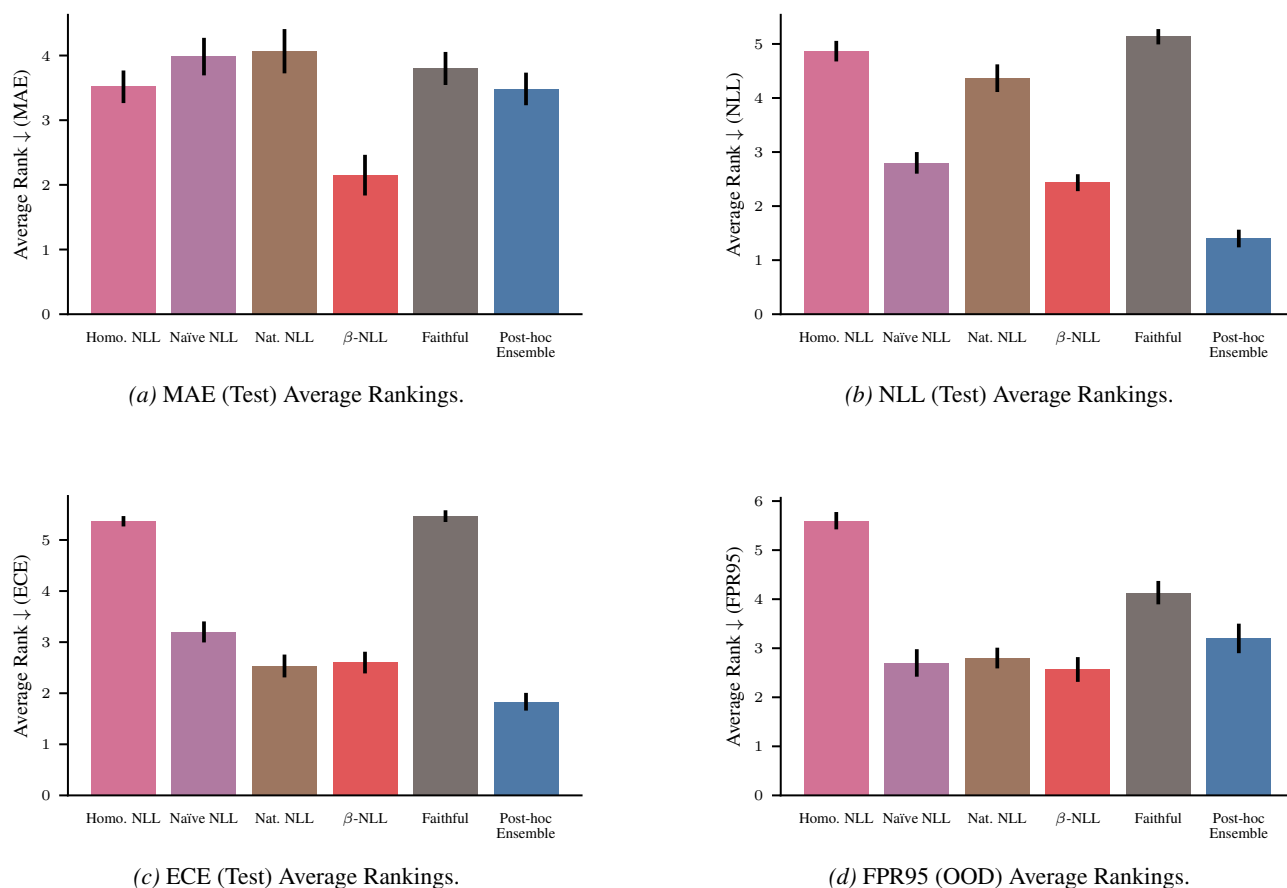


Figure 8. Additional rankings of methods on QM9. Rankings are computed for every combination of target and seed and averaged. Error bars indicate the standard error of the mean.

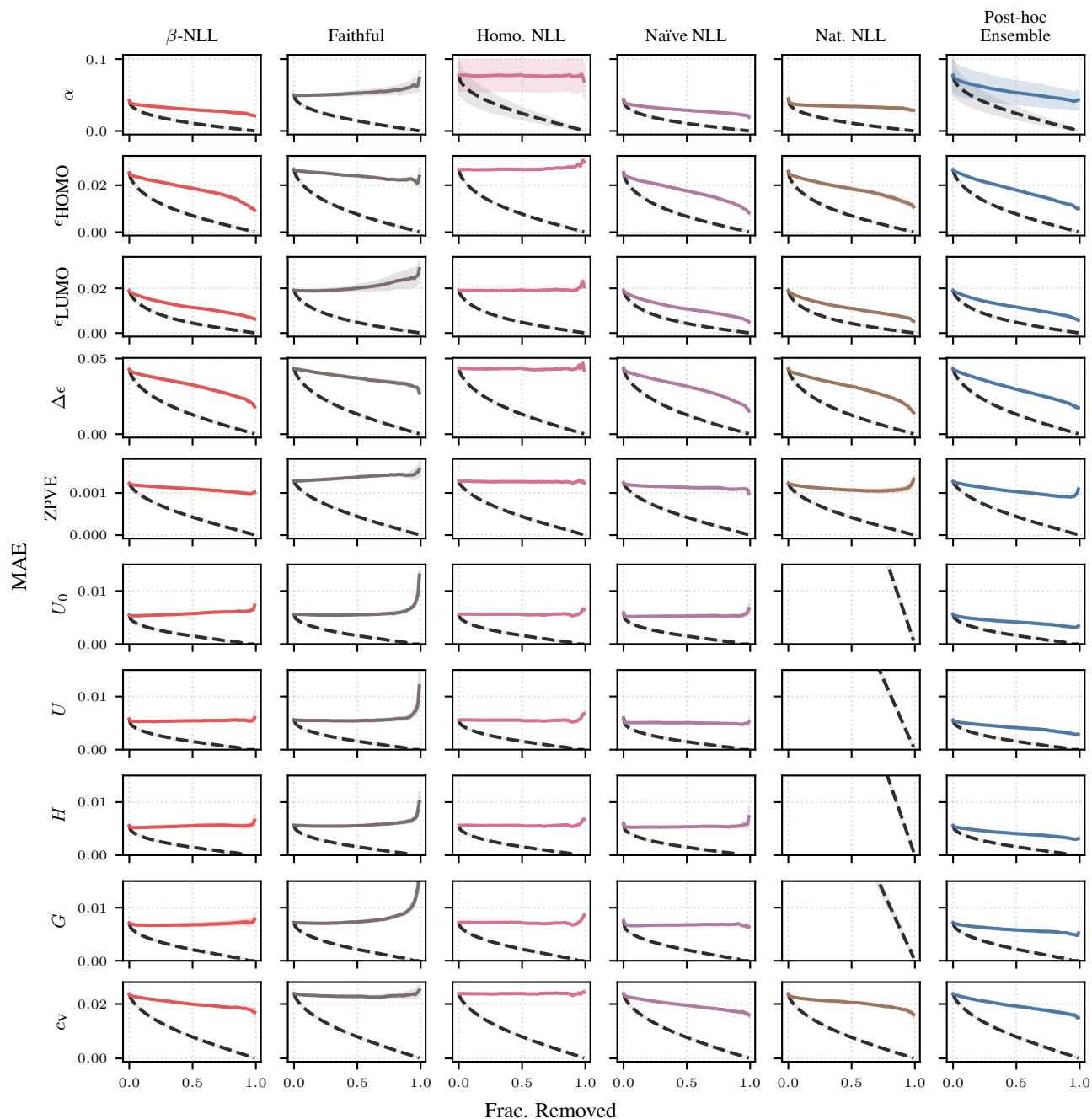


Figure 9. Calibration plots for each method for each target with average and one standard error of the mean. Plots are generated using the test set by ordering all predictions by variances and removing most uncertain points one-by-one (left side of plot with all datapoints, right side of plot with single most certain datapoint). The dotted lines are oracle lines for each model - these are created by ordering the predictions by their true residual and performing a similar procedure to obtain the full line. These indicate the calibration plot that would be obtained if the true residual was predicted. We note that the Natural NLL methods do not appear in the plots for targets  $U_0$ ,  $U$ ,  $H$  and  $G$  due to their numerical instability, and therefore it would not be possible to see the remaining methods if the y-axis was scaled to include these methods.

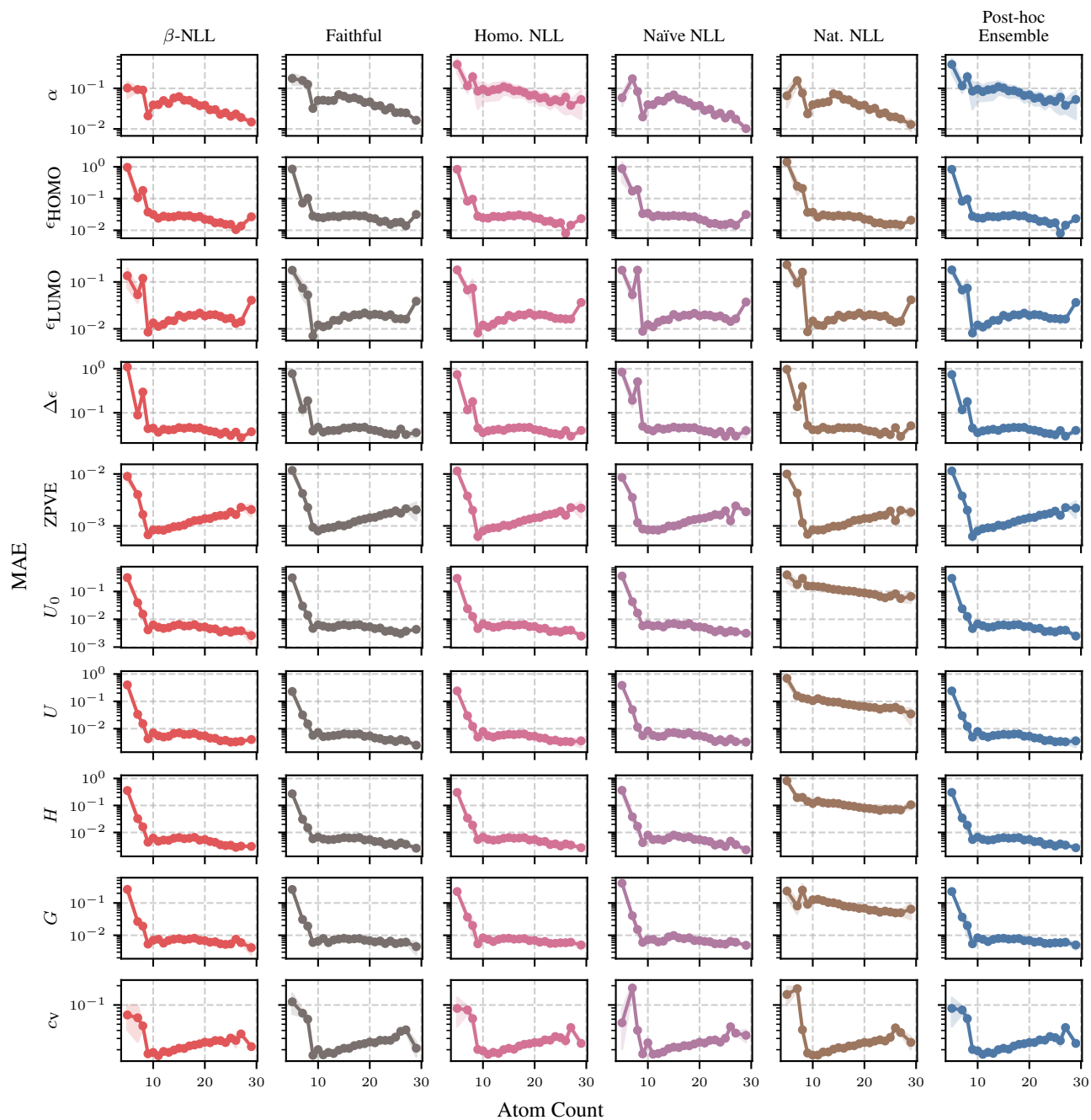


Figure 10. MAE as function of atom count of system for all methods on 10 targets from QM9. Means are presented with standard errors over three seeds.

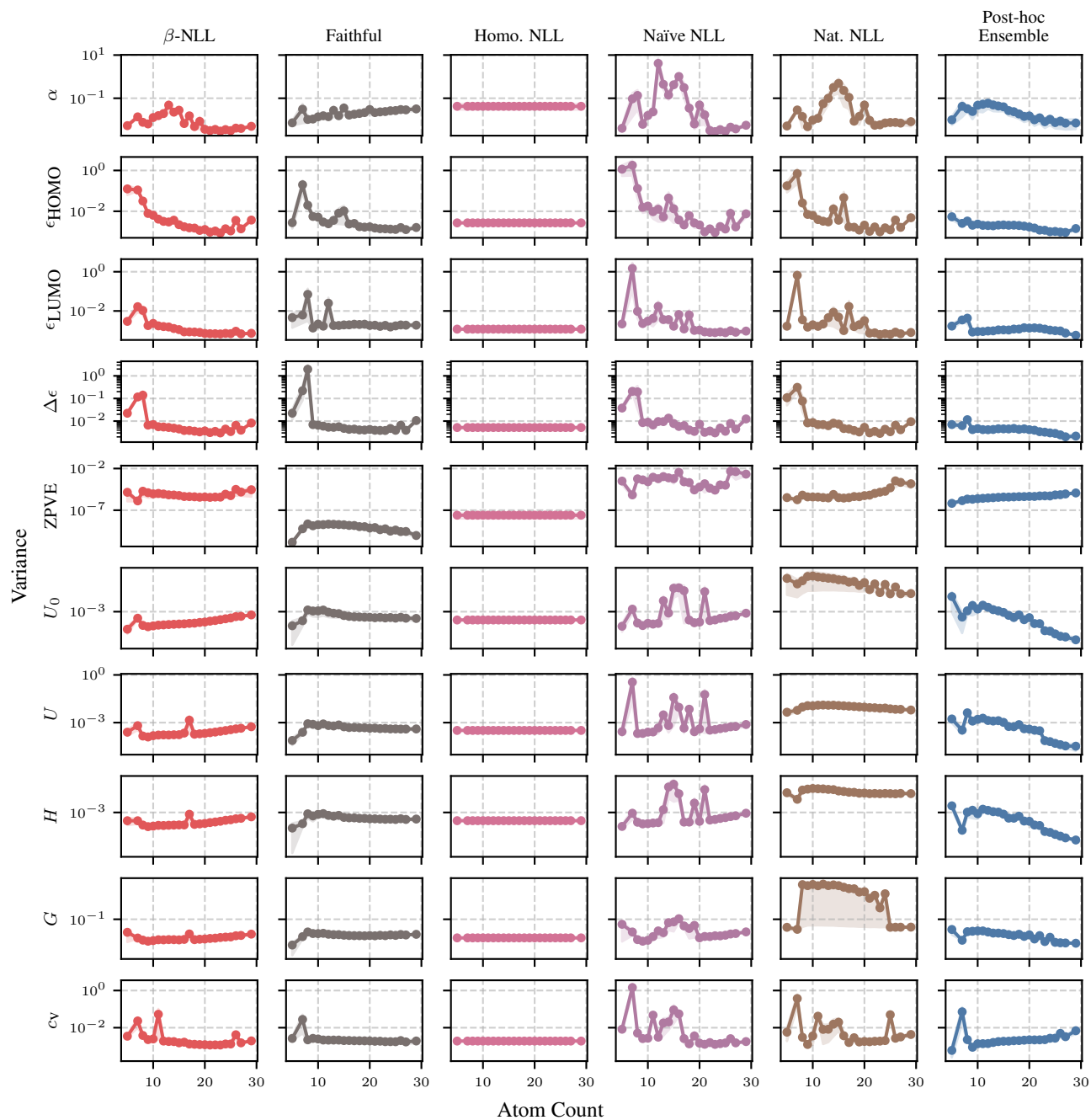


Figure 11. Variance as function of atom count of system for all methods on 10 targets from QM9. Means are presented with standard errors over three seeds.

## Practical Deep Heteroskedastic Regression

*Table 3.* Out-of-distribution (OOD) results for the models trained on QM9. In-distribution (ID) data is the test split of QM9 and the OOD data is a subset of the Alchemy dataset with the same number of datapoints as the ID data. The methods’ variance functions are used to discriminate between ID and OOD data and the metrics reported are the false positive rate at a 95% true positive rate (FPR95) and the area under the receiver operating characteristic curve (AUROC). Results are averages over three seeds with best results highlighted in bold font. The standard error of the mean is reported in parenthesis in the unit of the last significant digit.

Target	FPR95 ↓						AUROC ↑					
	Homo. NLL	Naïve NLL	Nat. NLL	$\beta$ -NLL	Faithful	Post hoc (Ensemble)	Homo. NLL	Naïve NLL	Nat. NLL	$\beta$ -NLL	Faithful	Post hoc (Ensemble)
$\alpha$	0.950 (0)	0.541 (27)	0.682 (190)	<b>0.498</b> (47)	0.624 (108)	0.696 (74)	0.500 (0)	0.835 (4)	0.848 (61)	<b>0.853</b> (15)	0.821 (65)	0.763 (34)
$\epsilon_{\text{HOMO}}$	0.950 (0)	0.882 (142)	0.868 (184)	0.865 (255)	0.992 (13)	<b>0.573</b> (123)	0.500 (0)	0.680 (120)	0.686 (133)	0.708 (198)	0.399 (267)	<b>0.867</b> (44)
$\epsilon_{\text{LUMO}}$	0.950 (0)	0.780 (27)	0.741 (8)	0.749 (31)	<b>0.676</b> (87)	0.756 (31)	0.500 (0)	0.720 (6)	0.740 (13)	0.741 (22)	<b>0.752</b> (43)	0.725 (43)
$\Delta\epsilon$	0.950 (0)	0.938 (67)	0.830 (145)	0.834 (252)	0.944 (48)	<b>0.476</b> (168)	0.500 (0)	0.698 (161)	0.763 (122)	0.679 (268)	0.654 (128)	<b>0.893</b> (52)
ZPVE	0.950 (0)	0.768 (66)	0.716 (147)	0.678 (45)	0.875 (78)	<b>0.666</b> (62)	0.500 (0)	0.760 (34)	0.792 (36)	0.809 (31)	0.556 (62)	<b>0.812</b> (26)
$U_0$	0.950 (0)	<b>0.384</b> (47)	0.749 (141)	0.454 (58)	0.818 (54)	0.827 (71)	0.500 (0)	<b>0.914</b> (11)	0.638 (154)	0.895 (21)	0.649 (30)	0.709 (62)
$U$	0.950 (0)	0.365 (29)	0.675 (34)	<b>0.358</b> (25)	0.784 (31)	0.814 (31)	0.500 (0)	0.919 (10)	0.754 (60)	<b>0.922</b> (8)	0.701 (42)	0.706 (20)
$H$	0.950 (0)	<b>0.353</b> (33)	0.594 (165)	0.403 (82)	0.784 (157)	0.805 (41)	0.500 (0)	<b>0.925</b> (8)	0.738 (82)	0.907 (22)	0.702 (122)	0.723 (33)
$G$	0.950 (0)	<b>0.572</b> (46)	0.599 (82)	0.600 (70)	0.784 (63)	0.814 (32)	0.500 (0)	<b>0.821</b> (20)	0.744 (105)	0.819 (32)	0.681 (80)	0.706 (14)
$c_v$	0.950 (0)	0.483 (283)	<b>0.127</b> (78)	0.616 (140)	0.744 (176)	0.231 (49)	0.500 (0)	0.895 (87)	<b>0.973</b> (12)	0.860 (48)	0.796 (78)	0.958 (11)

*Table 4.* Negative log-likelihood (NLL) for the baseline methods on QM9 before recalibrating them on the hold-out data by fitting a constant variance scale factor.

Target	NLL ↓			
	Naïve NLL	Nat. NLL	$\beta$ -NLL	Faithful
$\alpha$	127 (81)	11.2 (3)	11.6 (116)	47.7 (185)
$\epsilon_{\text{HOMO}}$	281 (340)	264 (195)	62.0 (278)	164 (141)
$\epsilon_{\text{LUMO}}$	212 (92)	346 (109)	81.4 (66)	417 (173)
$\Delta\epsilon$	172 (92)	169 (105)	66.0 (454)	85.3 (518)
ZPVE	-4.49 (6)	-4.56 (15)	-4.38 (24)	-4.12 (9)
$U_0$	28.5 (68)	1.15 (50)	30.1 (113)	27.2 (33)
$U$	27.8 (136)	1.47 (8)	31.4 (132)	24.7 (98)
$H$	42.9 (399)	1.12 (20)	28.9 (30)	26.8 (111)
$G$	31.1 (53)	1454 (2846)	15.5 (111)	27.4 (104)
$c_v$	31.5 (112)	10.4 (11)	18.5 (84)	21.3 (73)

### C. Additional Latent Representation Results - QM9

In this section of the appendix we provide additional results and analysis related to the sensitivity and ablation studies we perform to investigate the efficacy of our method and the effect of using different latent representations for the variance predictors. In Figure 12 we showcase rankings of the ECE on test set, and FPR95 and AUROC on the OOD set. We additionally present the raw metrics for each target in Tables 5 and 6. For all metrics, we note that last layers  $z^3$  and  $z^4$  generally perform the worst with  $z^0$  being third worst indicating that some level of feature learning must occur to properly predict variances. In terms of NLL, we note that the ensemble is the best, but for all other metrics we see that the "All" combination performs the best - we discuss this in Section 5. Finally, we also note that some seeds have very standard errors for some specific targets indicating a strong degree of overfitting; however, the ensembling procedure appears to mitigate this problem. In Fig. 14 we showcase calibration plots for each of the versions of our method for each target. Here we again note that all versions except for those solely relying on  $z^3$  or  $z^4$  have heuristically good calibration.

We then present additional results related to and sensitivity experiments on our method. Firstly, we present an additional weight decay experiment in Figure 15 where we again note that only  $z^3$  and  $z^4$  are very sensitive to the choice of weight decay, whilst the ensemble again is the most robust. In Figure 13 we show the sensitivity of each variation of our method to number of hold-out datapoints used to fit the variance heads. Here it is clear that many of the versions are highly sensitive to the size of the hold-out dataset, except for the ensemble which consistently performs extremely well which also was noticed when comparing to the other baselines.

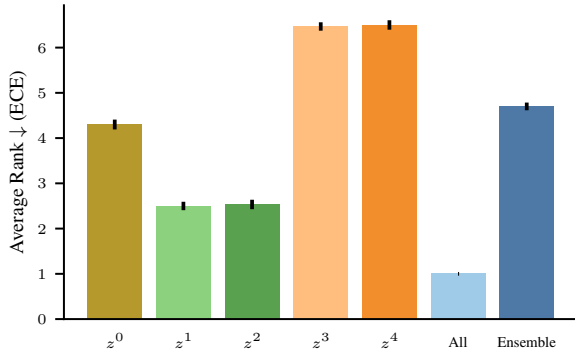
Table 5. Result of varying the latent representation  $z^l$  used for variance prediction in Eq. (7). The metrics shown are the test negative log-likelihood (NLL) and expected calibration error (ECE). Values are computed as means across three seeds with one standard error reported in parenthesis in the unit of the last significant digit. Best mean values are bolded.

Target	NLL ↓						ECE ↓							
	$z^0$	$z^1$	$z^2$	$z^3$	$z^4$	All	Ensemble	$z^0$	$z^1$	$z^2$	$z^3$	$z^4$	All	Ensemble
$\alpha$	-0.542 (458)	1.42 (439)	0.088 (298)	-0.775 (404)	-0.715 (424)	-0.573 (160)	<b>-1.04</b> (59)	0.038 (17)	0.026 (12)	0.022 (11)	0.042 (21)	0.068 (35)	<b>0.012</b> (4)	0.039 (19)
$\epsilon_{\text{HOMO}}$	-1.83 (3)	-1.86 (2)	-1.78 (2)	-1.74 (7)	1.22 (391)	-1.94 (1)	<b>-1.96</b> (1)	0.039 (1)	0.033 (2)	0.032 (3)	0.045 (0)	0.043 (3)	<b>0.016</b> (2)	0.038 (1)
$\epsilon_{\text{LUMO}}$	-1.97 (16)	-2.14 (3)	-2.13 (3)	-2.11 (3)	-2.07 (4)	-2.24 (4)	<b>-2.30</b> (2)	0.054 (2)	0.047 (0)	0.048 (2)	0.063 (4)	0.061 (1)	<b>0.024</b> (0)	0.054 (1)
$\Delta\epsilon$	-1.35 (5)	-1.37 (5)	-1.36 (4)	-1.35 (5)	38.2 (772)	-1.44 (1)	<b>-1.48</b> (1)	0.033 (3)	0.029 (1)	0.029 (2)	0.036 (3)	0.035 (3)	<b>0.014</b> (2)	0.032 (2)
ZPVE	-4.94 (3)	-4.96 (2)	-4.94 (3)	-4.83 (4)	-4.79 (1)	<b>-4.98</b> (2)	-4.97 (3)	0.029 (3)	0.023 (2)	0.025 (2)	0.049 (7)	0.049 (3)	<b>0.013</b> (2)	0.035 (2)
$U_0$	-2.94 (43)	-3.08 (30)	-3.37 (4)	-2.72 (58)	-0.838 (3599)	-3.22 (17)	<b>-3.46</b> (4)	0.056 (12)	0.033 (2)	0.032 (5)	0.111 (33)	0.121 (18)	<b>0.019</b> (3)	0.069 (5)
$U$	-3.06 (16)	-2.00 (209)	-3.17 (22)	-2.79 (16)	-2.67 (25)	-2.37 (145)	<b>-3.45</b> (3)	0.054 (2)	0.037 (3)	0.034 (2)	0.104 (25)	0.123 (16)	<b>0.020</b> (2)	0.070 (8)
$H$	-3.12 (7)	-3.14 (33)	-3.15 (32)	-2.88 (3)	-1.86 (131)	-1.20 (423)	<b>-3.46</b> (4)	0.050 (2)	0.035 (3)	0.035 (3)	0.106 (31)	0.113 (30)	<b>0.022</b> (2)	0.067 (9)
$G$	-3.02 (3)	-3.10 (3)	-2.87 (16)	-2.65 (21)	-1.16 (128)	-3.10 (10)	<b>-3.16</b> (4)	0.052 (5)	0.036 (5)	0.037 (4)	0.100 (24)	0.107 (19)	<b>0.023</b> (4)	0.067 (6)
$c_v$	-1.96 (6)	-2.01 (2)	-1.98 (2)	-1.84 (3)	-1.32 (106)	<b>-2.07</b> (1)	-2.04 (1)	0.032 (6)	0.027 (1)	0.032 (9)	0.067 (7)	0.065 (5)	<b>0.013</b> (4)	0.044 (3)

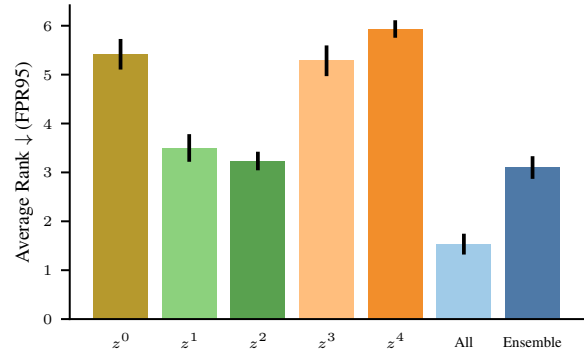
Table 6. Effect of the representation  $z^l$  used for linear variance prediction on OOD metrics. Values are computed as means across three seeds with one standard error reported in parenthesis in the unit of the last significant digit. Best mean values are bolded.

Target	FPR95 ↓						AUROC ↑							
	$z^0$	$z^1$	$z^2$	$z^3$	$z^4$	All	Ensemble	$z^0$	$z^1$	$z^2$	$z^3$	$z^4$	All	Ensemble
$\alpha$	0.878 (75)	0.776 (16)	0.702 (97)	0.761 (29)	0.757 (58)	<b>0.587</b> (120)	0.696 (74)	0.611 (137)	0.725 (39)	0.779 (51)	0.751 (31)	0.731 (22)	<b>0.840</b> (58)	0.763 (34)
$\epsilon_{\text{HOMO}}$	0.811 (43)	0.658 (136)	0.642 (155)	0.691 (254)	0.868 (114)	<b>0.464</b> (423)	0.573 (123)	0.679 (66)	0.817 (58)	0.815 (58)	0.778 (139)	0.650 (259)	<b>0.867</b> (140)	0.867 (44)
$\epsilon_{\text{LUMO}}$	0.859 (10)	0.769 (14)	0.755 (18)	0.808 (100)	0.829 (42)	<b>0.621</b> (38)	0.756 (31)	0.657 (24)	0.716 (84)	0.725 (27)	0.663 (89)	0.600 (54)	<b>0.823</b> (49)	0.725 (43)
$\Delta\epsilon$	0.849 (43)	0.816 (58)	0.529 (170)	0.586 (195)	0.684 (240)	<b>0.410</b> (147)	0.476 (168)	0.668 (64)	0.739 (58)	0.871 (65)	0.843 (76)	0.814 (89)	<b>0.913</b> (39)	0.893 (52)
ZPVE	0.805 (38)	0.746 (29)	0.718 (64)	0.874 (32)	0.790 (80)	0.712 (5)	<b>0.666</b> (62)	0.741 (41)	0.782 (21)	0.783 (27)	0.602 (41)	0.666 (75)	<b>0.821</b> (27)	0.812 (26)
$U_0$	0.850 (56)	0.704 (50)	0.710 (57)	0.900 (64)	0.911 (41)	<b>0.620</b> (31)	0.827 (71)	0.685 (31)	0.780 (40)	0.779 (44)	0.590 (128)	0.627 (81)	<b>0.845</b> (12)	0.709 (62)
$U$	0.839 (57)	0.677 (43)	0.747 (47)	0.917 (31)	0.893 (31)	<b>0.628</b> (56)	0.814 (31)	0.682 (36)	0.785 (22)	0.765 (22)	0.567 (101)	0.616 (55)	<b>0.847</b> (14)	0.706 (20)
$H$	0.815 (55)	0.699 (31)	0.747 (84)	0.877 (45)	0.899 (55)	<b>0.664</b> (13)	0.805 (41)	0.701 (40)	0.777 (18)	0.762 (49)	0.627 (78)	0.584 (116)	<b>0.829</b> (3)	0.723 (33)
$G$	0.737 (82)	0.729 (40)	0.775 (36)	0.887 (94)	0.908 (19)	<b>0.713</b> (84)	0.814 (32)	0.742 (71)	0.756 (12)	0.746 (12)	0.624 (137)	0.585 (36)	<b>0.811</b> (20)	0.706 (11)
$c_v$	0.681 (3)	0.639 (6)	0.348 (191)	0.610 (270)	0.724 (158)	0.268 (233)	<b>0.231</b> (49)	0.820 (14)	0.841 (18)	0.932 (41)	0.851 (95)	0.797 (87)	0.952 (40)	<b>0.958</b> (11)

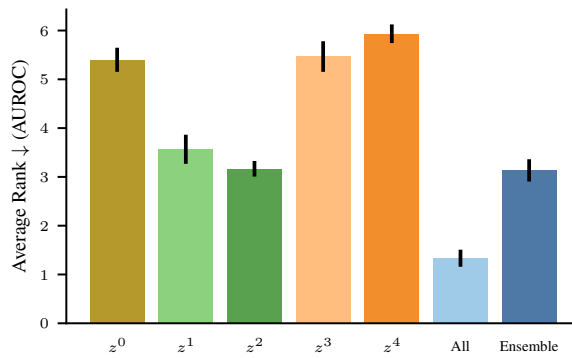
## Practical Deep Heteroskedastic Regression



(a) ECE (Test) Rankings for different representation usage.



(b) FPR95 (OOD) Rankings for different representation usage.



(c) AUROC (OOD) Rankings for different representation usage.

Figure 12. Additional rankings when using different latent representations or combinations thereof on QM9. Rankings are computed for every combination of target and seed, and then averaged with standard error of the mean.

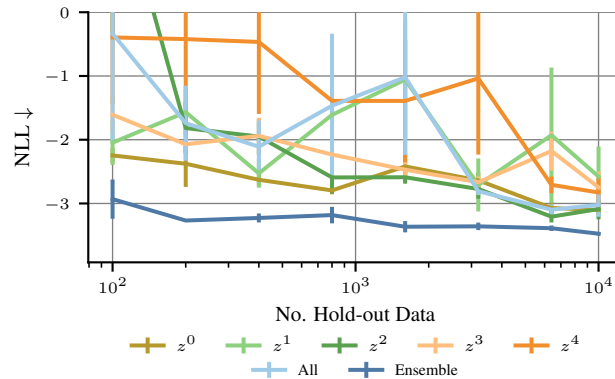


Figure 13. Effect of varying hold-out dataset size. Means are computed as averages across 3 repetitions and reported with one standard error of the mean.

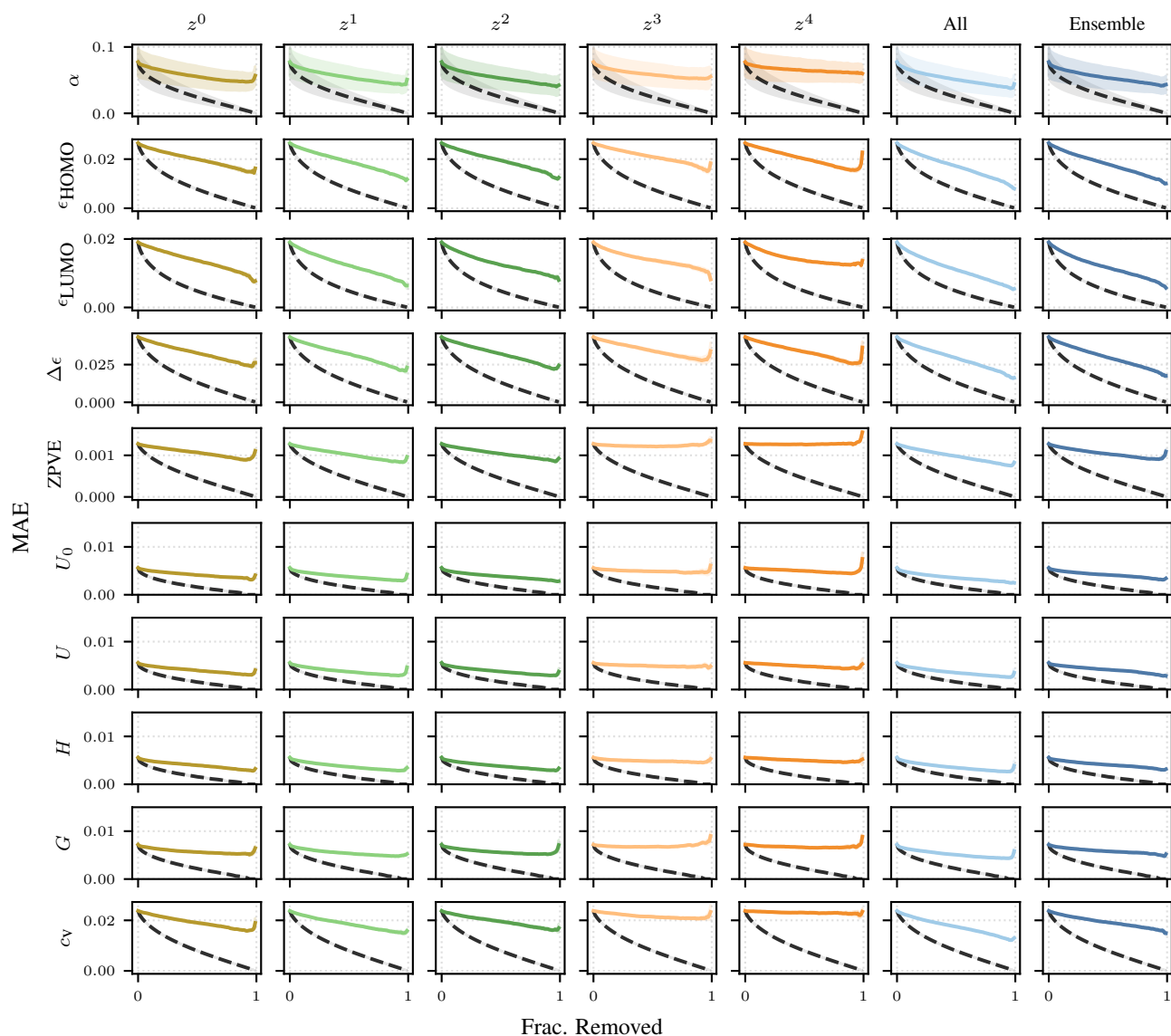


Figure 14. Calibration plots for each latent representation or combination thereof for each of the 10 targets on QM9. Each curve mean is computed over three seeds with one standard error of the mean shown. Plots are generated using the test set by ordering all predictions by variances and removing most uncertain points one-by-one (left side of plot with all datapoints, right side of plot with single most certain datapoint). The dotted lines are oracle lines for each model - these are created by ordering the predictions by their true residual and performing a similar procedure to obtain the full line. These indicate the calibration plot that would be obtained if the true residual was predicted.

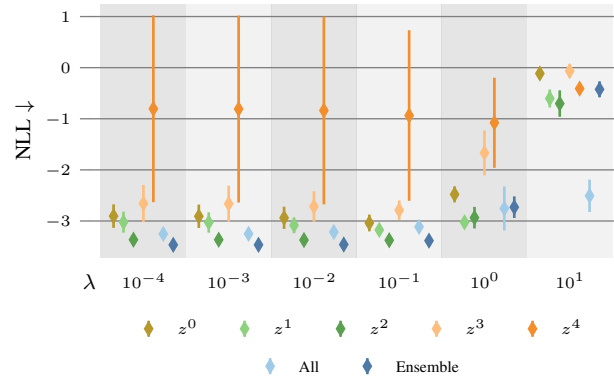


Figure 15. The effect of varying the weight decay parameter  $\lambda$  when fitting the linear uncertainty estimator using different individual representations  $z^l$ , all representations, or an ensemble of the individual estimators. Results are test NLL averages over three seeds on the QM9  $U_o$  target and are plotted with one standard error.

### D. Additional Results & Analysis - OMol25

In this part of the appendix we provide additional results and plots related to the OMol25 experiments. In Figure 18 and Figure 16 we provide calibration plots for UMA and AllScAIP variance heads respectively. In UMA we clearly again see how later representations provide worse calibrated uncertainties than earlier layers, with "All" and the ensemble performing even better. Interestingly we find that this pattern does not repeat for AllScAIP as corroborated by the calibration plots, where "All" peerforms the best, although with minor differences to the other method versions. This is further corroborated by Figure 17 where we showcase the NLL when using each different latent representation or combination thereof. Here we can see that several representations provide very strong NLLs, indicating that perhaps the latent representations throughout AllScAIP are less collapsed.

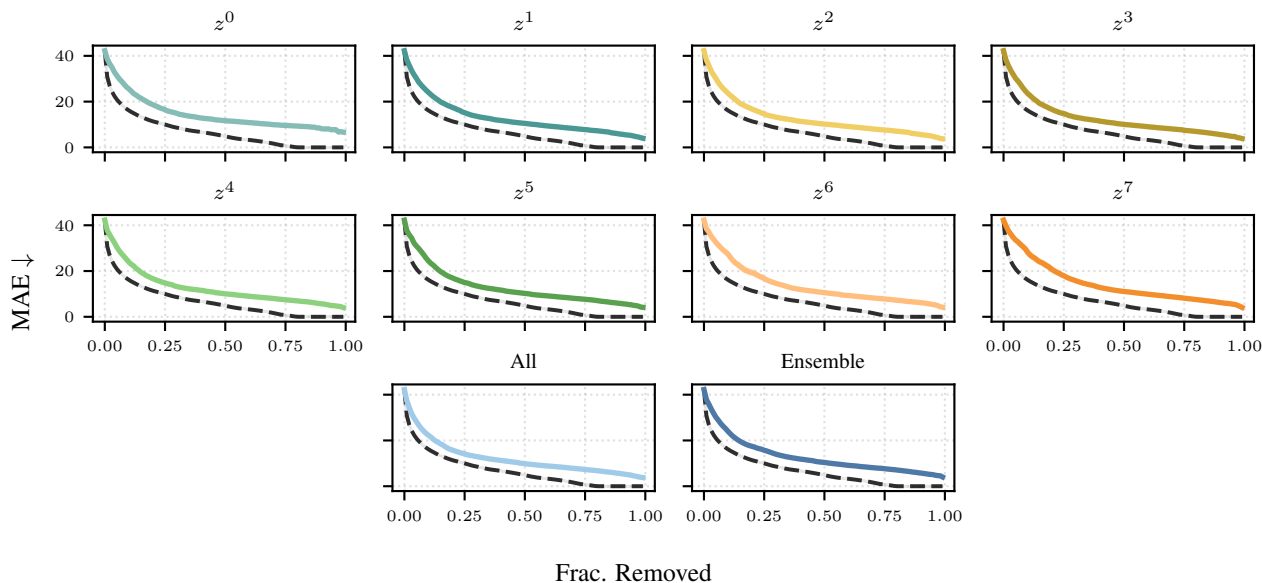


Figure 16. Calibration plots for each representation using AllScAIP on OMol25. Each curve mean is computed over three seeds with one standard error of the mean shown. Plots are generated using the test set by ordering all predictions by variances and removing most uncertain points one-by-one (left side of plot with all datapoints, right side of plot with single most certain datapoint). The dotted lines are oracle lines for each model - these are created by ordering the predictions by their true residual and performing a similar procedure to obtain the full line. These indicate the calibration plot that would be obtained if the true residual was predicted.

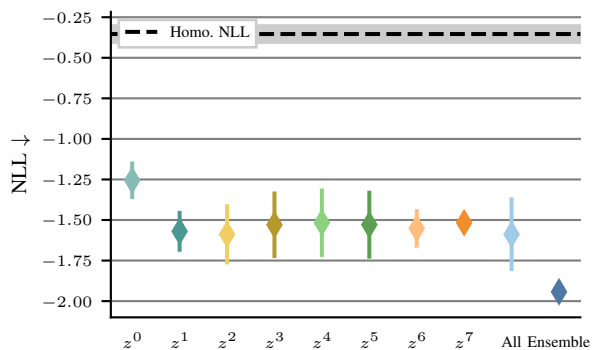


Figure 17. OMol25 test NLL when fitting the linear variance estimator using different individual representations  $z^l$ , all representations, or an ensemble of the individual estimators. Results are averages over three seeds and subsets of the full data. Error bars indicate the standard error of the mean.

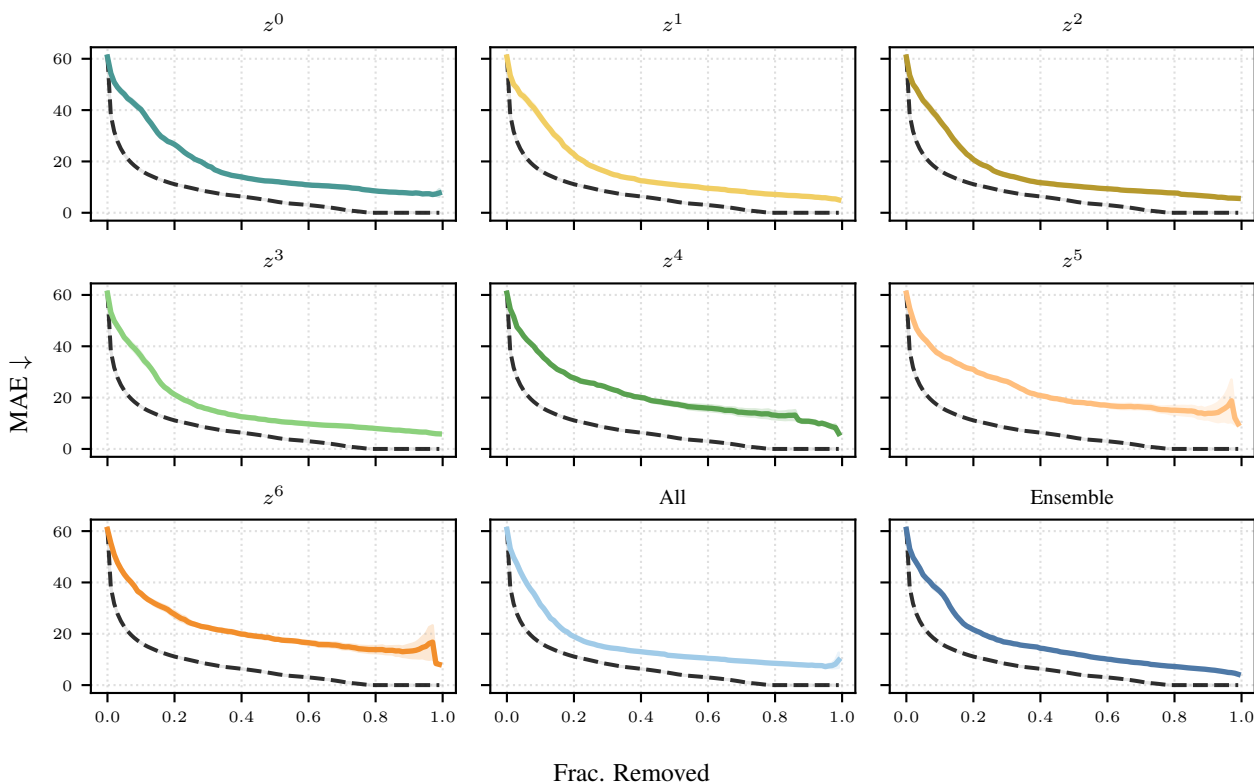


Figure 18. Calibration plots for each representation using UMA on OMol25. Each curve mean is computed over three seeds with one standard error of the mean shown. Plots are generated using the test set by ordering all predictions by variances and removing most uncertain points one-by-one (left side of plot with all datapoints, right side of plot with single most certain datapoint). The dotted lines are oracle lines for each model - these are created by ordering the predictions by their true residual and performing a similar procedure to obtain the full line. These indicate the calibration plot that would be obtained if the true residual was predicted.

## E. On Differences to Jimenez & Katzfuss 2025b

Here we elaborate on the differences to Jimenez & Katzfuss (2025b). In their work, the authors propose using Vecchia Gaussian Process ensembles on latent representations of neural networks trained for mean estimation only in regression tasks, using latent representation collapse as their motivation. Their method is post hoc, and relies on using GPs on all the latent representations throughout a neural network to predict both mean and uncertainty. The authors use training points as conditioning points for all the GPs, and due to the cubic cost of predicting with GPs, use Vecchia conditioning sets to reduce computational complexity. Vecchia conditioning sets are found at inference time by computing  $k$  nearest neighbors (where  $k$  is a hyperparameter) amongst the training data points for each latent representation  $\{z_1, \dots, z_L\}$ . In other words, at inference time their method requires computing  $k$  nearest neighbors  $L$  times and then conditioning  $L$  GPs on these conditioning sets, which is cubic in the number of conditioning points. These  $L$  GP predictive posteriors are then combined using a weighted product of predictive densities, where the weighting strategy is an additional hyperparameter choice. This adds up to 3 additional hyperparameter choices that must be made. Finally, their method relies on storing *all* training data such that it can be used at inference time for conditioning, which is not possible for large scale neural networks. The authors mention that using inducing-point GPs or a validation set in place of the training set could remedy this, but never investigate it (and again this would introduce another hyperparameter).

To conclude, we argue that whilst Jimenez & Katzfuss (2025b) were the first to use pretrained intermediate representations for UQ in regression, the additional hyperparameter choices makes their method significantly more difficult to use in practice than ours, and that the inference time and storage costs incurred by their method limits the applicability of their method in very large scale neural networks - especially in applications such as molecular dynamics where the model often must be called 500,000 to 1,000,000 times for a 1-nanosecond simulation. Moreover, it is not clear how their method would be used on graph neural networks for molecular property prediction, where features are obtained per atom. In contrast, our method

simply becomes a sum of the variance contributions computed for each atom as outlined in Eq. 12. At a minimum, their method would require significant changes to fit the setting of large scale neural networks and molecular property prediction.